University of Otago

RESEARCH REPORT

The Role of $G\alpha_{12/13}$ in CB_1-Mediated β-arrestin Recruitment

Steven A. Simpson

A thesis submitted in partial fulfilment of the Degree of
Bachelor of Biomedical Sciences with Honours.
University of Otago, Dunedin, New Zealand

October 2023

Acknowledgements

Firstly, I would like to thank my supervisor, Professor Michelle Glass, without whom this project would not have been possible. I greatly appreciate the opportunity to be part of your lab this year. I've thoroughly enjoyed being a part of your research team and learning from your vast knowledge in this field of research. Thank you for your encouragement and support this year, I greatly appreciate and am grateful for your expertise and guidance.

Also, a special mention to Gabriel Rawcliffe, Monica Patel, and Hayley Green, thank you for all your help throughout the year. I greatly value your time and patience in answering all my many questions and for guiding me in the lab. Thank you for supporting me and believing in my ability in the lab; I have learnt a great deal this year from you all.

To the Glass Lab group – those previously mentioned, Shuli Chen, Beth Ryalls, Nadia Kuepper, Tasmin Turner-Thomas, and Ian Liddle; thank you for making me feel welcome and for your friendship throughout the year. I've enjoyed learning from you all this year and thank you for your generous and ongoing encouragement.

To my friends both in the pharmacology department and outside, thank you for your support and encouragement throughout the year. I appreciate your friendship greatly.

To my parents, Helen and David Simpson, and my sisters, Melissa and Steffi, thank you so much for believing in and encouraging me this year, and all those prior. Thank you for listening to all my science facts throughout the year and encouraging me to keep going when things got difficult. I love you all.

Abstract

The main psychoactive ingredient in the plant *Cannabis sativa* is Δ^9-*trans*-tetrahydrocannabinol, which was found to signal through the cannabinoid CB_1 receptor (CB_1). CB_1 is one of two main G protein-coupled receptors (GPCRs) in the endocannabinoid system. Though CB_1 has been shown to preferentially couple to $G\alpha_{i/o}$ proteins, there has been evidence for promiscuous coupling to other classes. $G\alpha_{12/13}$ proteins are one of the four main families of G proteins and act through Rho-guanine nucleotide exchange factors to stimulate RhoA. This leads to the activation of Rho-associated kinase and regulation of the actomyosin cytoskeleton. To modulate the signalling of GPCRs, arrestins have been demonstrated to have a key role in governing the processes of internalisation and desensitisation. Here, this research aimed to investigate the role of $G\alpha_{12/13}$ proteins in the modulation of CB_1-mediated β-arrestin recruitment. In HEK293A wild type (WT) cells, CB_1 activated both $G\alpha_{12}$ and $G\alpha_{13}$ proteins in a concentration-dependent manner in TRUPATH G protein dissociation bioluminescence resonance energy transfer (BRET) assays. CB_1-mediated β-arrestin 2 recruitment was enhanced in a concentration-dependent manner in HEK293A $G\alpha_{12/13}$ protein knock-out ($\Delta G\alpha_{12/13}$) cells, compared to WT cells in BRET β-arrestin translocation assays. β-arrestin 2 recruitment was almost abolished with the reintroduction of $G\alpha_{12/13}$ proteins. Phosphorylation of extracellular-signal regulated kinase was assessed using a BRET biosensor assay, showing attenuated levels in $\Delta G\alpha_{12/13}$ cells compared to WT cells, which was not restored when adding back $G\alpha_{12/13}$ proteins. Receptor trafficking revealed no differences in cell surface half-life of CB_1 between WT and $\Delta G\alpha_{12/13}$ cells, though the addition of β-arrestin reduced half-life in both cell lines. Interestingly, the morphology of $\Delta G\alpha_{12/13}$ cells appeared to have more cytoskeletal outgrowths than WT cells, which was reversed when $G\alpha_{12/13}$ proteins were reintroduced. Overall, we demonstrate that $\Delta G\alpha_{12/13}$ proteins are activated at CB_1, though their modulatory role on CB_1-mediated β-arrestin recruitment requires further study.

Table of Contents

List of Figures

List of Tables

List of Abbreviations

AMB	AMB-FUBINACA
BRET	Bioluminescence resonance energy transfer
BSA	Bovine serum albumin
cAMP	3', 5'- Cyclic adenosine monophosphate
CB_1	Cannabinoid CB_1 receptor
$\Delta G\alpha_{12/13}$	$G\alpha_{12/13}$ knock-out
DMEM	Dulbecco's modified Eagle medium
EC_{50}	Concentration at which response is half-maximum
EDTA	Ethylenediaminetetraacetic acid
EKAR	Extracellular signal-regulated kinase activity reporter
ERK	Extracellular signal-regulated kinase
FBS	Foetal bovine serum
G Protein	GTP binding protein
GFP	Green fluorescent protein
GPCR	G protein-coupled receptor
GRK	G protein coupled receptor kinase
GTP	Guanosine-5'-triphosphate
GTPase	GTP hydrolase enzyme
HEK 293	Human embryonic kidney 293 cells
NEV	NLuc-EKAR-Venus
NLuc	Nanoluciferase
PBS	Phosphate buffered saline
PDL	Poly-D-lysine
PEI-Max	Polyethyleneimine Max
pERK	Phosphorylated ERK
PFA	Paraformaldehyde
PKA	Protein kinase A
Rho-GEF	Rho guanine nucleotide exchange factor
RLuc8	Renilla luciferase 8
ROCK	Rho-associated protein kinase
SEM	Standard error of the mean
SFM	Serum-free Medium
THC	Δ^9-tetrahydrocannabinol
WT	Wild type
YFP	Yellow fluorescent protein
ZCZ	ZCZ-011

1 Introduction

The plant *Cannabis sativa* has been extensively used and consumed historically for a range of purposes, including for medicinal applications (Pisanti & Bifulco, 2019). However, the main psychoactive ingredient in *Cannabis* was not fully discovered until 1964, being identified as Δ^9-*trans*-tetrahydrocannabinol (THC) (Gaoni & Mechoulam, 1964). Subsequently, investigation into this phytocannabinoid found that within the body it signalled predominantly through two main G protein coupled receptors (GPCRs). The endocannabinoid system was discovered to be comprised of endogenous receptors, endogenous cannabinoids and their synthesis and degradation enzymes, which are found in many areas (Bisogno et al., 1999). These receptors were the cannabinoid CB_1 and cannabinoid CB_2 receptors (CB_1 and CB_2, respectively). CB_1 and CB_2 are found in a variety of regions throughout the body (Matsuda et al., 1990; Munro et al., 1993). CB_1 is highly localised in brain regions involved in motor control and cognition, highlighting the role of the endocannabinoid system in these functions (Glass et al., 1997). CB_2 was found to be predominantly located in the periphery and immune cells (Munro et al., 1993).

1.1 G protein Coupled Receptors

1.1.1 Cannabinoid Receptor 1

When THC was first discovered, its mechanism of action was unknown, with the prevailing theory being that cannabinoids caused lipid perturbations upon intercalation in membranes. This was thought to change the activity or binding characteristics of neurotransmitters and hormones (Hillard et al., 1985; Howlett, 1985). However, this theory was challenged by Howlett et al., (1986) who reported THC inhibited adenylate cyclase (AC) in a pertussis toxin-sensitive (G protein-specific) manner (Dolby & Kleinsmith, 1974; Howlett et al., 1986). This

led to the conclusion that THC targets a $G\alpha_{i/o}$ linked GPCR. This was supported by the successful cloning of a brain-derived cannabinoid-responsive GPCR from rat cDNA, now known as CB_1 (Matsuda et al., 1990). CB_1 (like CB_2) is part of the Class A rhodopsin-like family of receptors. Like all GPCRs, CB_1 has a structure comprised of seven trans-membrane alpha helices connected via loops with an extracellular N-terminus and an intracellular C-terminus (Matsuda et al., 1990).

1.1.2 Cannabinoid Ligands

Since the discovery of CB_1, many endogenous and exogenous ligands have been found to target this GPCR, which are grouped into several cannabinoid ligand classes. A typical agonist is a ligand which binds in the orthosteric site on the receptor, causing the receptor to change conformation to a more active state. Different agonists can have varying efficacies, with 'full' agonists producing maximal responses and 'partial' agonists producing less than maximal effects. The two endogenous ligands for CB_1 are anandamide (AEA) and 2-arachidonylglycerol (2-AG), which bind to the orthosteric site. Other ligands include plant-based phytocannabinoids, such as THC, and a wide range of synthetic cannabinoid receptor agonists (SCRAs). AMB-FUBINACA (AMB) is a particularly potent and efficacious SCRA (Banister et al., 2016; Gamage et al., 2018). In comparison, THC has a much lower efficacy than AMB (Finlay et al., 2019), despite both binding to the orthosteric binding site (Finlay et al., 2019; Hua et al., 2017; Krishna Kumar et al., 2019). Alongside these orthosteric ligands, there are those that bind to an alternative (allosteric) ligand binding site. Allosteric ligands can be allosteric modulators or allosteric agonists, which alter the affinity or efficacy of orthosteric ligands, or activate the receptor directly (Kenakin, 2007). 'Pure' allosteric modulators only alter the receptor activation in the presence of an orthosteric agonist (Kenakin, 2007). However, allosteric agonists like ZCZ-011 (ZCZ) are able to produce some agonist-like effects without

an orthosteric agonist bound (Gentry et al., 2015; Green et al., 2022; Ignatowska-Jankowska et al., 2015).

1.1.3 G protein Activation

The guanine nucleotide binding protein (G protein) consists of three subunits: α, β and γ, which exist as a GDP-bound heterotrimer when inactive. When a ligand binds to the GPCR, a conformational change occurs affecting helices 3 and 6, causing the unmasking of G protein binding sites (Hamm, 1998). The receptor acts as a guanine nucleotide exchange factor (GEF)

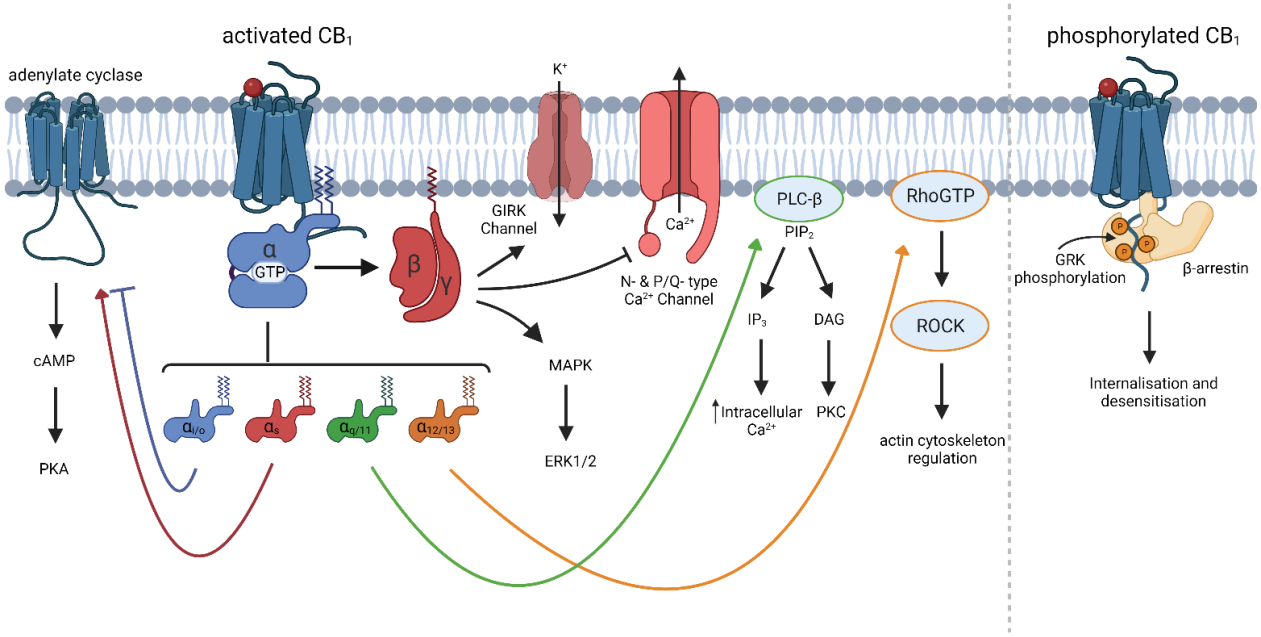

Figure 1. Overview of CB_1 Signalling Pathways.
Upon ligand binding, CB_1 couples predominantly to $G\alpha_{i/o}$ proteins, which act to inhibit adenylate cyclase (AC) and the production of cAMP, also lowering protein kinase A (PKA) activity. Additionally, the βγ subunit causes activation of mitogen-activated kinase (MAPK), leading to the phosphorylation of extracellular signal-regulated kinase (ERK1/2). CB_1 has also been shown to couple to $G\alpha_s$, which leads to activation of AC, as well as activating $G\alpha_{q/11}$ proteins which stimulate phospholipase C (PLC) and protein kinase C (PKC). Though indirect, there has been evidence linking CB_1 to $G\alpha_{12/13}$, which acts through Rho-associated kinases (ROCK) to regulate the actin cytoskeleton. CB_1 also modulates the activity of inwardly rectifying K^+ channels (GIRK) and N and P/Q type Ca^{2+} channels. G protein receptor kinases (GRKs) phosphorylate CB_1 leading to recruitment of β-arrestins, which regulate receptor internalisation and desensitisation. Figure created with Biorender.com.

and facilitates the exchange of GDP for GTP (guanine nucleotides) (Duc et al., 2015). This triggers the dissociation of the Gα and Gβγ subunits, causing the initiation of their downstream signalling pathways. G proteins are categorized according to their Gα-subunit type, of which there are four main families: $G_{i/o}$, G_s, $G_{q/11}$ and $G_{12/13}$. Each G protein family interacts with a distinct set of second messengers and are grouped according to their sequence homology and the signalling cascades they initiate.

1.2 G protein Signalling

The activation of G proteins leads to the subsequent triggering of downstream effector cascades (Figure 1). The $G\alpha_s$ and $G\alpha_{i/o}$ families of G proteins are linked to the activation and inhibition of AC, respectively. The $G\alpha_{q/11}$ proteins have been linked to the activation of phospholipase C, while the $G\alpha_{12/13}$ family have been shown to be involved in GTPase (GTP hydrolase enzyme) and Rho signalling pathways (Neves et al., 2002).

1.2.1 $G\alpha_{i/o}$ Signalling

CB_1 is canonically linked to the $G\alpha_{i/o}$ family of G proteins, with multiple studies showing CB_1 causes inhibition of AC (Bayewitch et al., 1995; Bidaut-Russell et al., 1990; Felder et al., 1992; Howlett, 1985; Matsuda et al., 1990). Pertussis toxin (PTX) leads to the inhibition of $G\alpha_{i/o}$ proteins through selective adenosine-diphosphate ribosylation (Neves et al., 2002). Thus, as the linkage between CB_1 and AC pathways was PTX-sensitive, it was concluded that the receptor must couple to this family of G proteins (Howlett, 1985; Howlett et al., 1986). The inhibition of AC leads to a decrease in intracellular cyclic AMP (cAMP) and subsequent decrease in the activity of protein kinase A (PKA) (Bidaut-Russell et al., 1990; Howlett et al., 1986). Furthermore, cAMP has a modulatory effect on not only PKA, but also on phosphodiesterases and ion channels (Antoni, 2012). In addition, agonist activation of CB_1 has been shown to

inhibit calcium channels, including P/Q-type and N-type channels (Mackie et al., 1995; Mackie & Hille, 1992; Sugiura et al., 1996). CB_1 stimulation has also been reported to activate inwardly rectifying potassium channels (Mackie et al., 1995), leading to hyperpolarisation of the membrane in which they are located, reducing the likelihood of synaptic transmission.

1.2.2 $G\alpha_s$ Signalling

The $G\alpha_s$ family of G proteins have a stimulatory effect on AC activity, which leads to an increase in cAMP concentration, as well as increasing PKA activity. Though CB_1 is widely accepted to be $G\alpha_i$-coupled, there has been evidence of a $G\alpha_s$ linkage. The inactivation of $G\alpha_i$ proteins using PTX revealed a receptor-mediated increase in cAMP (Glass & Felder, 1997; Kearn et al., 2005). In addition to this finding, similar patterns in cAMP accumulation have been seen in other studies, which used a variety of cell types including CHO (Chinese hamster ovary) and HEK (Human Embryonic Kidney) (Bonhaus et al., 1998; Calandra et al., 1999; Felder et al., 1998; Finlay et al., 2017). Here, it was suggested that $G\alpha_i$ protein signalling could become exhausted, by either CB_1 overexpression (Finlay et al., 2017) or by co-stimulating the dopamine type 2 receptor (Glass & Felder, 1997; Kearn et al., 2005). In the absence of sufficient $G\alpha_i$ the receptor couples to $G\alpha_s$ suggesting that $G\alpha_s$ proteins bind to CB_1 with lower affinity than $G\alpha_i$.

1.2.3 $G\alpha_{q/11}$ Signalling

The $G\alpha_{q/11}$ family of G proteins are a class of proteins which stimulate the membrane-bound enzyme phospholipase C (PLC), which converts phosphatidylinositol 4,5-bisphosphate (PIP_2) into breakdown products inositol triphosphate (IP_3) and diacylglycerol (DAG) (Neves et al., 2002). Whilst DAG activates protein kinase C (PKC), IP_3 activates a ligand-gated calcium channel on the endoplasmic reticulum, releasing calcium into the cytoplasm, resulting in the

activation of calcium-dependent pathways (Syrovatkina et al., 2016). $G\alpha_{q/11}$ proteins have been reported to couple to CB_1, observed through increases in PLC-specific cytosolic calcium concentrations when stimulated with WIN55,212-2, a high efficacy synthetic ligand, in both HEK cells transfected with CB_1 and hippocampal neurons (Lauckner et al., 2005). Here, the increase in cytosolic calcium was insensitive to PTX, but was blocked with the addition of CB_1 antagonist SR141716A. THC and 2-AG were able to produce similar PLC-dependent enhancement of intracellular calcium in neuroblastoma cells (Sugiura et al., 1997). However, Lauckner et al., (2005) did not report a comparable trend with these agonists in HEK cells. Another study concluded that both anandamide and WIN55,212-2 were unsuccessful in activating PLC through CB_1 in Chinese Hamster Ovary (CHO) cells (Felder et al., 1995). Taken together, this evidence seems to suggest that there are cell-dependent, and agonist specific effects involved with CB_1 coupling to $G\alpha_{q/11}$.

1.2.4 $G\alpha_{12/13}$ Signalling

The $G\alpha_{12/13}$ family of G proteins are linked to the regulation of the cytoskeleton, among other downstream effects, and were first discovered in 1991 – the last of the families to be defined (Strathmann & Simon, 1991). $G\alpha_{12/13}$ protein activity is modulated by regulators of G protein signalling (RGS) proteins. The RGS proteins which govern $G\alpha_{12/13}$ protein signalling are the Rho-guanine nucleotide exchange factors (RhoGEFs) (Kozasa et al., 1998). The RhoGEFs that are known to bind to $G\alpha_{12/13}$ proteins are p115-RhoGEF, PDZ-RhoGEF, leukaemia-associated RhoGEF (LARG) and Lbc-RhoGEF (Dutt et al., 2004; Fukuhara et al., 1999; Kozasa et al., 1998). $G\alpha_{12/13}$ binding stimulates the GEF activity of the RhoGEFs, causing the exchange of GDP and GTP, through stimulation of small GTPase RhoA (Sah et al., 2000). RhoA activity is also governed by Rho-guanine nucleotide dissociation inhibitors (Rho-GDIs), which inactivate RhoA through binding to the C-terminus (Fauré & Dagher, 2001). Once activated, RhoA has

several downstream effectors, including Rho-associated kinases (ROCK). ROCK activates focal adhesion kinase, which leads to the generation of actin stress fibres. This occurs through the serum response transcription factor (SRF) that binds to its respective response element (SRE) to regulate transcription (Buhl et al., 1995; Treisman et al., 1998). In addition, ROCK also phosphorylates the myosin light chain (MLC) proteins, inducing cellular contraction (Narumiya et al., 1997; Riento & Ridley, 2003).

$G\alpha_{12/13}$ proteins are known to couple to a wide range of GPCRs, including muscarinic M_3 (Rümenapp et al., 2001), lysophosphatidic acid (LPA) (Gohla et al., 1998), thromboxane (TXA_2) (Offermanns et al., 1994), sphingosine-1-phosphate (Sugimoto et al., 2003) and protease-activated receptors (Hains et al., 2006). However, there is only limited evidence demonstrating direct CB_1 coupling to $G\alpha_{12/13}$. A recent study created Bioluminescence Resonance Energy Transfer-based (BRET) Nanoluciferase Binary Technology (NanoBiT) biosensors to measure G protein dissociation and RhoA activation at a range of GPCRs, including CB_1 (Inoue et al., 2019). The NanoBiT sensor was a split-luciferase design, with the Large BiT (Lg) and the Small BiT (Sm) of the luciferase tagged onto separate effector proteins (Dixon et al., 2016). The Nanoluciferase enzyme is only active when the Lg and Sm parts of the enzyme are in close proximity and the coelenterazine substrate is present, allowing for detection of G protein dissociation or RhoA activity. Here, the study identified that CB_1, but not CB_2 induced activation of the $G\alpha_{12/13}$ pathway through the NanoBiT RhoA sensor upon stimulation with CP-55940 (Inoue et al., 2019). A previous study reported that anandamide was able to induce neuroblastoma cell rounding via a ROCK-sensitive pathway, as the response was inhibited in the presence of ROCK inhibitor Y-27632 (Ishii & Chun, 2002). Furthermore, another study demonstrated that CB_1 was linked to the contraction of the actomyosin cytoskeleton via the ROCK pathway, which was prevented through the administration of rat $G\alpha_{12/13}$-targeted siRNAs (Roland et al., 2014). Thus, Roland et al., (2014) proposed that $G\alpha_{12/13}$

proteins were necessary for actomyosin contraction through CB_1. Overall, these studies demonstrated that $G\alpha_{12/13}$ signalling pathways are linked to CB_1 but provided only limited evidence of direct G protein-receptor coupling.

1.2.5 Gβγ Signalling

Though the Gα subunit is thought to mediate the major signalling responses of GPCRs, the Gβγ subunit has also shown to be important in intracellular signalling (Dupré et al., 2009). There are a few key effectors which are regulated by Gβγ. The G protein regulated inwardly rectifying potassium channels (GIRKs), as well as N or P/Q -type calcium channels, are stimulated by Gβγ heterodimers (Khan et al., 2013). Furthermore, the Gβγ subunit has also been demonstrated to display a regulatory role of G protein receptor kinases (GRKs), phospholipases and some adenylate cyclases (Khan et al., 2013). Gβγ proteins have also been shown to phosphorylate mitogen-activated protein kinase (MAPK) and extracellular signal-related kinases (ERK1/2).

1.2.6 Extracellular signal-related kinase Signalling

Extracellular signal-related kinase 1/2 (ERK1/2) signalling is a key pathway in controlling cell proliferation, migration and differentiation, as well as having other roles (Lavoie et al., 2020). The activation (phosphorylation) of ERK1/2 is controlled by a wide range of intracellular signals, including G protein signalling. The activation of GPCR signalling can cause the activation of the Raf kinases, through Akt and Ras (Jain et al., 2018). Subsequently, Raf kinases phosphorylate MAPK/ERK1/2 kinases (MEKs), which is the penultimate step in the cascade of activating ERK1/2 through phosphorylation (Morrison, 2012). In addition to Ras and Akt pathways, GPCR signalling can also cause ERK1/2 activation through other pathways such as through cAMP and PKA (Kearn et al., 2005). CB_1 has been shown to be linked to increased ERK1/2 activity in CHO cells, which was PTX-sensitive ($G\alpha_{i/o}$-linked) (Bouaboula et al., 1995;

Kearn et al., 2005). In contrast, other evidence has shown that, despite PTX-sensitivity, the CB_1-mediated pERK response was not dependent on cAMP in both CHO cells and in neurons (Bouaboula et al., 1995; Derkinderen et al., 2001). This suggested that pERK production was regulated by a different mechanism, potentially by the Gβγ subunit acting to recruit Akt (Galve-Roperh et al., 2002; Gómez Del Pulgar et al., 2000; Laprairie et al., 2014). In addition, the regulation of ERK1/2 has also been discovered to act through the Src family of non-receptor tyrosine kinases (Derkinderen et al., 2003; Ibsen et al., 2017).

1.2.7 β-arrestin Signalling

Alongside typical G protein mediated signalling, GPCRs can recruit other proteins through which they signal. A key class of proteins are the β-arrestins (1 and 2, also known as arrestin-2 and -3, respectively), which have a regulatory role for GPCRs (DeWire et al., 2007). A number of studies have demonstrated interactions between both the β-arrestins and CB_1 (Daigle et al., 2008; Jin et al., 1999; Manning et al., 2023). Here, GPCR kinases (GRKs) phosphorylate serine and threonine residues on the C-terminal of GPCRs, creating a distinct phosphorylation barcode (Nobles et al., 2011). The barcode generated through GRK activity then drives the recruitment of β-arrestins (Delgado-Peraza et al., 2016). Both β-arrestin 2 and GRK3 have been shown to be important in the internalisation of CB_1 (Jin et al., 1999). β-arrestin 2 has a role in the formation of clathrin-coated vesicles, which act to engulf the receptor facilitating the process of endocytosis (Daigle et al., 2008; Hsieh et al., 1999). CB_1 is degraded following phosphorylation and internalisation, unlike some other GPCRs which may be recycled back to the cell surface (Grimsey et al., 2010).

In addition to regulating GPCR internalisation and degradation, β-arrestins are also implicated in the activation of ERK1/2 signalling, among other roles (Delgado-Peraza et al., 2016). There are several pathways which result in the phosphorylation of ERK1/2, though Gβγ and β-arrestin

2 have been shown to be particularly important (Laprairie et al., 2014). Additionally, further studies of ERK1/2 phosphorylation displayed a potential role for mediation by β-arrestin 1 (Ahn et al., 2013; Flores-Otero et al., 2014). However, the evidence is at times varied, proposing both Gα-specific (Gamage et al., 2016), Gβγ-specific (Bouaboula et al., 1995) and arrestin-specific ERK pathways (Ahn et al., 2013).

1.3 Research Aims

This research aims to investigate the relationship between CB_1 and $G\alpha_{12/13}$ proteins in the recruitment of β-arrestin. This research builds on pilot data from the Glass lab which suggested enhanced CB_1 mediated β-arrestin recruitment in $G\alpha_{12/13}$ knock-out HEK cells. Overall, the key hypothesis in this study is that $G\alpha_{12/13}$ proteins are key regulators in the recruitment of β-arrestin by CB_1. Firstly, the project will investigate if CB_1 can directly activate $G\alpha_{12/13}$. Three structurally distinct ligands (Δ^9-*trans*-tetrahydrocannabinol, AMB-FUBINACA and ZCZ-011) will be employed to determine if the ligands are able to differentially drive G protein activation and β-arrestin recruitment. Additionally, the functional downstream consequences of altered β-arrestin recruitment will be investigated. This research is divided into a few aims:

- Characterisation of $G\alpha_{12/13}$ activation at CB_1
    - To investigate whether $G\alpha_{12/13}$ proteins are directly activated by CB_1, a BRET-based G protein dissociation assay in Human Embryonic Kidney wild type (HEK) cells will be performed. CB_1 and BRET-tagged $G\alpha_{12}$ and $G\alpha_{13}$ proteins will be expressed, with the G protein activation measured in response to THC, AMB and ZCZ.

- Investigating the effect of $G\alpha_{12/13}$ proteins on CB_1-mediated β-arrestin recruitment
    - To study the effect of G protein expression on β-arrestin recruitment, a BRET-based β-arrestin membrane translocation assay will be employed, comparing CB_1

mediated arrestin recruitment in HEK wild type cells to HEK cells in which $G\alpha_{12/13}$ have been knocked-out. To test the specificity of the response, $G\alpha_{12/13}$ proteins will be reintroduced into knock-out cells, aiming to restore the response seen in wild type cells.

- Investigating the consequences of $G\alpha_{12/13}$ modulation of β-arrestin recruitment
    - The effect on ERK phosphorylation as a downstream effector will be assessed using a BRET-based pERK biosensor.
    - Receptor trafficking will be used to assess changes in both cell surface and total CB_1 expression, with the amount of internalisation measured using quantitative immunocytochemistry.
    - Immunocytochemistry will also be used to assess any morphological changes to cells with altered G protein expression.

The results from these experiments will enable the characterisation of not only $G\alpha_{12/13}$ activation at CB_1, but also the effect of $G\alpha_{12/13}$ protein expression on β-arrestin recruitment. In addition, these assays will help elucidate any functional consequences behind the pattern of β-arrestin recruitment seen with $G\alpha_{12/13}$ protein knock-out.

2 Methods

2.1 Cell Culture

2.1.1 Cell Lines

The Human Embryonic Kidney (HEK) 293A cell line has been widely used in the field of GPCR research, as they are easy to transfect and maintain. In this research, two HEK 293A cell lines were used:

- HEK 293A Wild Type (WT): Wild Type cell line, with no transgenes introduced (Thermo Fisher Scientific).
- HEK 293A $G\alpha_{12/13}$ knock-out ($\Delta G\alpha_{12/13}$): A stable HEK 293A cell line with the $G\alpha_{12/13}$ family of G proteins selectively removed using CRISPR/Cas9 techniques (Ran et al., 2013).

The WT and $\Delta G\alpha_{12/13}$ cell lines were generously gifted from Professor Hans Bräuner-Osborne (University of Copenhagen, Denmark) and from Professor Asuka Inoue (Tohoku University, Japan), respectively. For generation and validation of the $\Delta G\alpha_{12/13}$ cell line refer to Inoue et al., (2019).

2.1.2 Cell Maintenance and Resuscitation

Cells were resuscitated from cryo-storage in liquid nitrogen as needed. Each aliquot of cryopreserved cells was approximately 3 million cells/mL suspended in Dulbecco's Modified Eagle Medium (DMEM) with 10% FBS and 5% dimethyl sulfoxide (DMSO). Cells were quickly thawed in a water bath at 37 °C and added to 9 mL of fresh, warmed DMEM. The cell suspension was then centrifuged at 160 g for 5 minutes to form a cell pellet. The supernatant was discarded, and the cells were resuspended in 5 mL DMEM (+ 10% FBS) and placed in a

Corning® 25 cm^2 culture flask. Cells were then expanded to a 75 cm^2 flask once confluency had reached approximately 90%.

Cells were regularly monitored and passaged once confluency had reached 80-90% (every three to four days) in Corning® 75 cm^2 culture flasks. DMEM with 10% FBS was used to maintain cells. During passaging, medium was removed, prior to a wash with phosphate-buffered saline (PBS). Cells were then incubated for three to five minutes with 0.05% Trypsin-EDTA (Thermo Fisher Scientific) at 37 °C to lift cells from the flask. Fresh medium was added prior to trituration to break up clusters of cells and obtain single cell suspension. A fraction of cells was then deposited back into the flask, with the rest used for seeding assays or discarded. The fraction of replaced cells depended on the desired length of time between passages and how quickly the cells grew. For HEK293A WT cells this was either 1:12 or 1:15 and for HEK293A $\Delta G\alpha_{12/13}$ cells either 1:10 or 1:12. Cells were cultured in a total volume of 5 mL or 10 mL medium for 25 cm^2 and 75 cm^2 flasks, respectively. Flasks were kept in an incubator at 37 °C with 5% CO_2.

2.1.3 Seeding and Transfection

Cell counts were obtained using a 1:2 dilution with Trypan Blue (Thermo Fisher Scientific) and counted with an automatic haemocytometer to determine the desired concentration (million per millilitre) for dilution prior to seeding. Depending on the nature and size of the experiment, cells were either seeded into 100 mm dishes or 6-well plates. Cells seeded onto Corning® 100 mm dishes were seeded at 2.5 x 10^6 or 1.5 x 10^6 for transfection 24 or 48 hours later, respectively. When seeding onto Corning® 6-well plates, cells were seeded at 0.5 x 10^6 or 0.26 x 10^6 for transfection 24 or 48 hours later, respectively. All dishes/plates were incubated at 37 °C with 5% CO_2. Seeded cells typically reached 50-80% confluency prior to transfection, which included a media change before a transfection mixture was added.

This transfection mixture comprised of two solutions:

1. DNA constructs relevant to the assay made up to 500 or 86.4 µL in Opti-MEM™ (for 100 mm or 6 well plate, respectively).
2. Polyethyleneimine-max (PEI-Max, Polysciences) at a ratio of 1:9 (DNA: PEI-Max) made up to 500 or 86.4 µL in Opti-MEM™.

The two transfection solutions were combined and incubated at room temperature for 20 minutes, before being added dropwise to cells in dishes/plates.

2.1.4 Plating of Cells

Approximately 24 hours following transfection, cells were lifted from the dishes/plates with trypsin as described in cell maintenance above. Cells were resuspended in DMEM (with 10% FBS) and then counted using an automatic haemocytometer, as in the seeding protocol above. Cells were diluted to varying concentrations based on experimental protocol (explained in each protocol below), between 200,000 -600,000 cells/mL. Cells were plated on either white opaque 96-well plates (Corning® Costar® or PerkinElmer CulturPlate™) or clear-bottom plates (Corning® Costar®). Prior to plating cells, 37 µL per well of 0.05 mg/mL poly-D-lysine (PDL, Sigma-Aldrich) was added and incubated for 40 minutes – 1 hour. PDL was collected after plate treatment and reused up to three times. PDL-treated wells were washed with 100 µL PBS prior to adding cells.

2.2 G protein Dissociation BRET Assay – TRUPATH

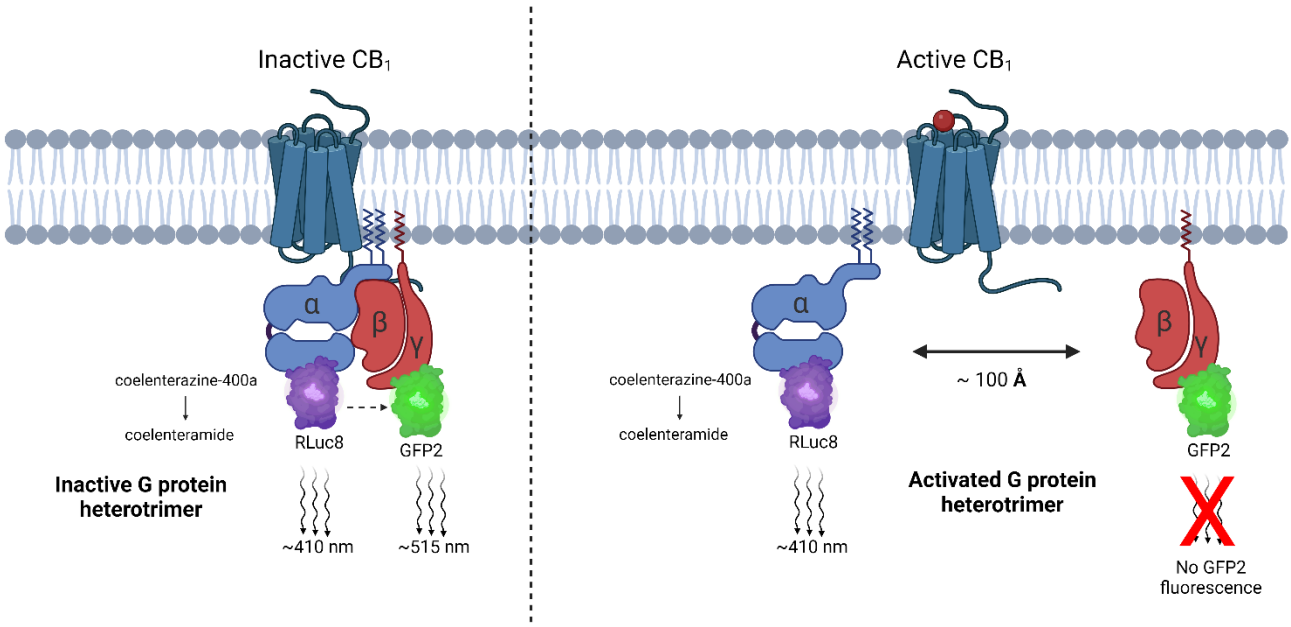

Figure 2. The TRUPATH BRET2 Assay.
Left) At rest, the G protein subunits are in an inactive heterotrimer state, meaning the RLuc8 donor and GFP2 acceptor are close enough for BRET to occur. **Right)** When CB_1 is activated, the G protein trimer activates and dissociates, pushing BRET donor and acceptor apart, causing decreasing fluorescence levels from GFP2. Figure created with Biorender.com.

The dissociation of $G\alpha_{12}$ and $G\alpha_{13}$ proteins at CB_1 was measured using the recently described TRUPATH Bioluminescence Resonance Energy Transfer 2 (BRET2) Assay (Olsen et al., 2020). TRUPATH is a collection of plasmids encoding BRET $G\alpha\beta\gamma$ biosensors, four of which were used in this research (tagged $G\alpha_{12}$/$G\alpha_{13}$, tagged $G\gamma_9$ and $G\beta_3$). These biosensors allow the measurement of G protein activation through dissociation of G protein subunits (Olsen et al., 2020). In the TRUPATH BRET assay (Figure 2), the Renilla-Luciferase-8 (RLuc8) donor is tagged onto the Gα-subunit and emits light from the breakdown of coelenterazine-400a into coelenteramide at approximately 410 nm. This light activates the green fluorescent protein-2 (GFP2) acceptor tag on the Gβγ-subunit, which then emits fluorescence at approximately 515 nm. The amount of light produced at 410 nm indicates the expression of RLuc8 in the cells and, therefore, is an indication of transfection efficiency. The amount of BRET fluorescence at 515

nm is directly linked to the proximity of the tags on the G protein subunits. Thus, the TRUPATH BRET assay allows the measurement of G protein activation. The data collected is expressed as a BRET ratio (515/410 nm) and is directly proportional to G protein dissociation.

For each TRUPATH BRET assay, the seeding, transfection, and plating of HEK293A WT cells were performed as described above. Cells seeded onto 10 cm dishes were transfected with a total of 3.75 μg of DNA construct consisting of four components:

- 1500 ng pplss-3HA-hCB$_1$ pEF4A
- 750 ng each of: Gβ_3 pcDNA3.1 and Gγ_9-GFP2 pcDNA3.1
- 750 ng of Gα_{12}-Rluc8 pcDNA5 or Gα_{13}-Rluc8 pcDNA5

Following approximately 24 hours of incubation, cells were plated at a density of 6 x 10^4 cells per well on white opaque 96-well CulturPlate^{TM} (PerkinElmer) plates which were PDL-treated (~40 minutes to 1 hour).

TRUPATH BRET2 assays were conducted in half plate reads (48 wells) or 'runs' in a LUMIstar® Omega (BMG Labtech GmbH, Ortenberg, Germany) plate reader, using 0.5 second detection per well. Reading only part of the plate helped to minimise the loss of kinetic data between measurements of a well. Prior to reading, media (DMEM + FBS) was aspirated, cells were washed with PBS, and medium replaced with 80 μL phenol red-free DMEM (with 1 mg/mL fatty acid-free Bovine Serum Albumin (BSA) and 10 mM HEPES). Plates were then incubated for 30 minutes. For each half plate read, cells were treated with 10 μL of Coelenterazine-400a at 5 μM (Nanolight Technologies) and luminescence was detected simultaneously for a 5-minute pre-read at 37 °C to establish a stable baseline reading. THC, ZCZ and AMB were prepared to 10x final concentration from stock aliquots kept at -80 °C and diluted in drug vehicle containing assay medium, absolute ethanol (1:100) and DMSO (1:100).

Following the pre-read, cells were stimulated with 10 µL of drug to make a final volume of 100 µL and were read for approximately 25 minutes. For both the pre-read and read, fluorescent emissions at 410 nm (RLuc8) and 515 nm (GFP2) were detected concurrently and recorded using the Omega Control software. BRET ratios (515/410 nm) were then exported using the Omega MARS software. GraphPad Prism v10 was used to graph and analyse data, producing kinetic time courses normalised to vehicle control. Area under the curve analysis was utilised to produce concentration-response curves from kinetic data, which was fitted using a three parameter, non-linear regression curve to obtain potency and efficacy parameters. Where normalising to vehicle control was not possible, data was normalised to the lowest drug concentration.

2.3 β-arrestin Translocation Assay

First characterized in 2015 (Donthamsetti et al., 2015), the β-arrestin translocation assay utilises a similar technique to the TRUPATH BRET assay, though this assay uses BRET1 rather than BRET2. The β-arrestin translocation assay measures the translocation of arrestin to the cell surface. In this assay, β-arrestin 2 is tagged with Nanoluciferase (NLuc), which breaks down coelenterazine-h into coelenteramide, producing luminescence at ~475 nm (Figure 3). Membrane-bound Citrine is tagged with Yellow Fluorescent Protein (YFP) and, when near, NLuc luminescence causes BRET to occur, producing light at approximately 535 nm. As with the RLuc8 luminescence, the amount of light at 475 nm indicates the amount of NLuc expressed. Once the receptor has been phosphorylated, β-arrestins are recruited to the receptor, bringing the NLuc tag closer to the membrane-bound Citrine increasing the fluorescence at 535 nm. Thus, the assay allows the measurement of β-arrestin translocation to the membrane as a proxy for β-arrestin recruitment to exogenously overexpressed receptors following agonist stimulation. Data in this assay is reported as a BRET ratio (535/475 nm) and is proportional to

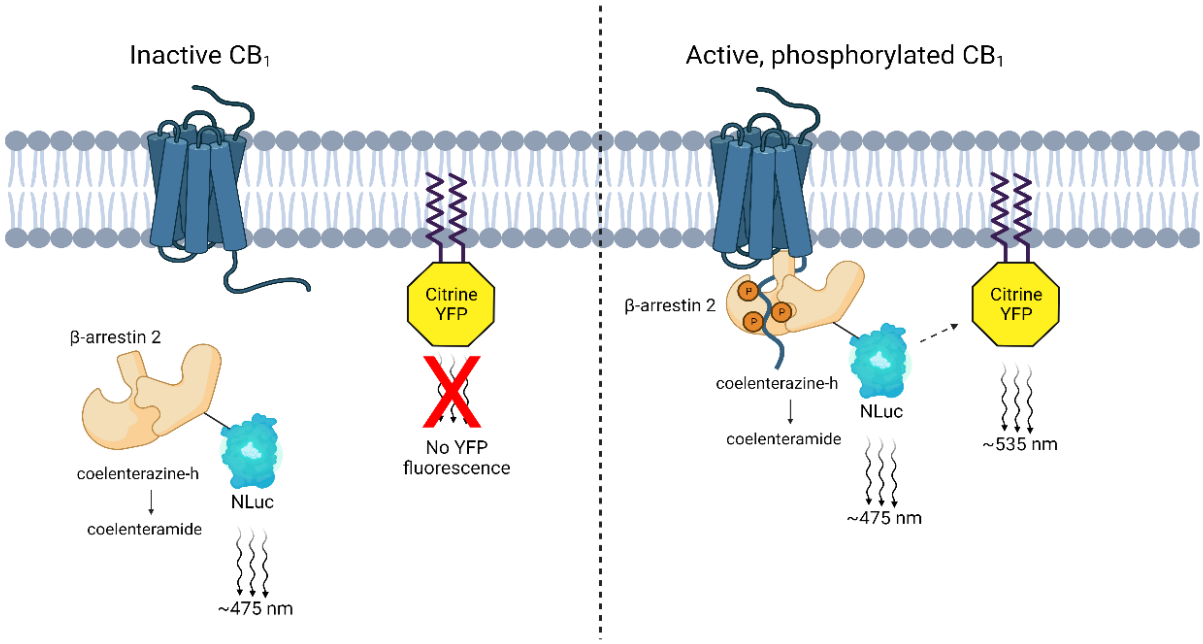

Figure 3. The β-arrestin Translocation BRET1 Assay.
Left) When the receptor is in an inactive state, there is no β-arrestin translocation, meaning no BRET occurs between the NLuc and Citrine tags. **Right)** Following agonist stimulation, the receptor is phosphorylated, initiating the recruitment of β-arrestin. β-arrestin is translocated to the membrane, bringing the BRET donor and acceptor tags close enough for BRET to occur, producing fluorescence at 535 nm. Figure created with Biorender.com.

the level of β-arrestin translocation.

For each assay, the seeding, transfection, and plating of HEK293A WT and HEK 293A $\Delta G\alpha_{12/13}$ cells were performed as described above. Cells seeded onto 6-well plates were transfected with the relevant four or five DNA constructs, depending on the condition:

- 260 ng pplss-3HA-hCB$_1$ pEF4A
- 345 ng mem-linker-citrine-SH3 pcDNA5
- 8.64 ng NLuc-hβ-arrestin-2 pcDNA3.1
- 130 or 260 ng Empty Vector pcDNA3.1
- 130 ng hGNA12 and/or 130 ng hGNA13 pcDNA5 (to ensure a total DNA of 874 ng/well)

Table 1 displays the transfection conditions used in the assay, with cell line type and whether the condition had hGNA12 and/or hGNA13 added back to the $\Delta G\alpha_{12/13}$ cells. Following approximately 24 hours of incubation, cells were plated at a density of 3 x 10^4 cells per well on white opaque 96-well CulturPlate™ (PerkinElmer) plates which were PDL-treated (~40 minutes to 1 hour).

Table 1. Transfection Conditions for β-arrestin Translocation Assay.
Plus/minus each construct is marked with '+/-'. For Empty Vector, one '+' represents 130 ng.

DNA Construct	WT Cells	$\Delta G\alpha_{12/13}$ cells	$\Delta G\alpha_{12/13}$ cells + $G\alpha_{12}$	$\Delta G\alpha_{12/13}$ cells + $G\alpha_{13}$	$\Delta G\alpha_{12/13}$ cells + $G\alpha_{12}$ + $G\alpha_{13}$
Mem-linker-Citrine-SH3	+	+	+	+	+
Pplss-3HA-CB_1	+	+	+	+	+
NLuc-hβ-Arrestin-2-Sp1	+	+	+	+	+
hGNA12	-	-	+	-	+
hGNA13	-	-	-	+	+
Empty Vector	++	++	+	+	-

β-arrestin BRET1 assays were conducted in half plate reads (48 wells) in a LUMIstar® Omega plate reader, using 0.35 second detection per well. Prior to reading, media was removed, cells were washed with PBS, and medium was replaced with 80 µL phenol red-free DMEM (1 mg/mL BSA, 10 mM HEPES). The plate was then serum starved for 30 minutes in the assaying medium. For each half plate read, cells were treated with 10 µL of Coelenterazine-h at 5 µM (Nanolight Technologies) and luminescence was detected simultaneously for a 5-minute pre-

read at 37 °C to establish a stable baseline reading. THC, ZCZ and AMB were prepared to 10x final concentration from stock aliquots kept at -80 °C and diluted in drug vehicle containing assay medium, absolute ethanol (1:100) and DMSO (1:100). Following the pre-read, cells were stimulated with 10 µL of drug to make a final volume of 100 µL and were read for approximately 25 minutes. For both the pre-read and read, fluorescent emissions at 475 nm (NLuc) and 535 nm (YFP) were detected concurrently and recorded using the Omega Control software. BRET ratios (535/475 nm) were then exported using the Omega MARS software. GraphPad Prism v10 was used to graph and analyse data, producing kinetic time courses normalised to vehicle control. Area under the curve analysis was utilised to produce concentration-response curves from kinetic data, which was fitted using a three parameter, non-linear regression curve to obtain potency and efficacy parameters.

2.4 pERK Assay

The pERK BRET reporter assay uses the same BRET principles as previously explained for G protein dissociation and β-arrestin translocation. However, rather than individual tags on separate proteins, the pERK biosensor is a single chain, with both BRET tags part of the protein. The biosensor has an extracellular signal-regulated kinase activity reporter (EKAR) region which was developed from the Cdc25C sequence and was originally designed as a FRET biosensor in 2008 (Harvey et al., 2008). The NLuc-EKAR-mVenus (NEV) biosensor used in this research contains an NLuc tag, which produces luminescence (475 nm) from the breakdown of coelenterazine-h as previously described. In the presence of pERK, the Cdc25C region is phosphorylated, allowing the Cdc25C to interact with the WW phospho-binding domain (Figure 4). The folding of the biosensor leads to the NLuc donor / mVenus acceptor pair being in close enough proximity for BRET to occur, producing light at 535 nm. Additionally, there is a nuclear-localising sequence in the WW domain, which can be exported

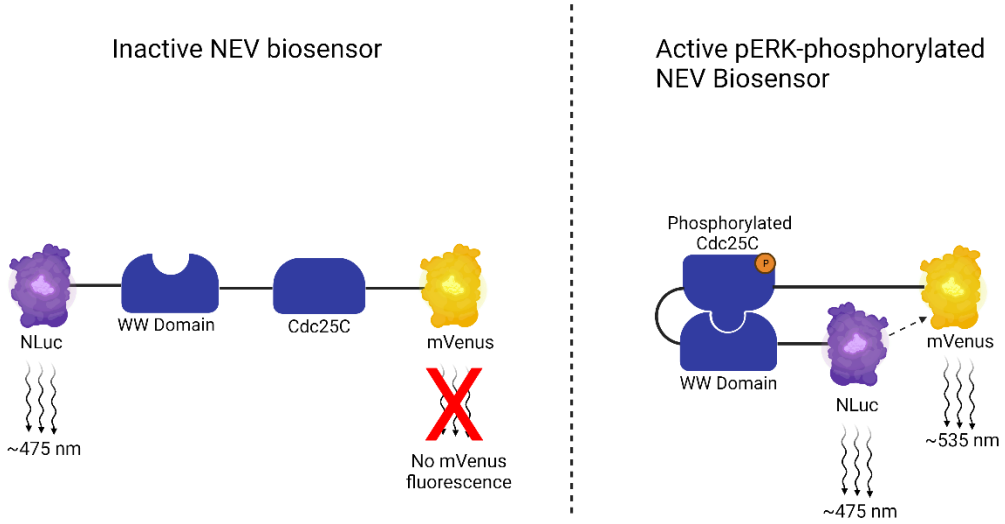

Figure 4. The pERK BRET1 Assay.
Left) Low levels / absence of pERK means the Cdc25C region is not phosphorylated, with the NLuc and mVenus too far apart for BRET to occur. **Right)** When pERK is present, the Cdc25C region is phosphorylated and binds to the WW domain, folding the biosensor and pushing BRET donor and acceptor closer, causing activation of mVenus. Figure created with Biorender.com.

from the nucleus with the expression of a secondary sequence, forming nuclear and cytoplasmic versions of the biosensor (Harvey et al., 2008). The data from this assay is expressed as a BRET ratio (535/475 nm) and is proportional to the amount of pERK present.

For each assay, the seeding, transfection, and plating of HEK293A WT and HEK 293A $\Delta G\alpha_{12/13}$ cells were performed as described above. Cells seeded onto 10 cm dishes or 6-well plates were transfected with the relevant DNA constructs, depending on the condition:

- 1600 ng pplss-3HA-hCB$_1$ pEF4A
- 50 ng NEV-Cytoplasmic pRK5
- 50 ng NEV-Nuclear pRK5
- 750 ng hGNA12 and/or 750 ng hGNA13 pcDNA5
- 800, 1550 or 2300 ng Empty Vector pcDNA3.1 (to ensure a total DNA of 4 µg/dish)

Table 2 displays the transfection conditions used for 10 cm dishes in the assay, with cell line type and whether the condition had hGNA12 and/or hGNA13 added back to the $\Delta G\alpha_{12/13}$ cells. Transfection amounts were scaled down by a factor of 5.79 from 10 cm dish values to account for lower 6-well plate area when appropriate. Following approximately 24 hours of incubation, cells were plated at a density of 3 x 10^4 cells per well on white opaque 96-well CulturPlate™ (PerkinElmer) or Costar® (Corning®) plates which were PDL-treated (~40 minutes to 1 hour). Plated cells were left for a minimum of 5 hours, before plating media was removed, cells were washed with PBS, and medium was replaced with 80 µL phenol red-free DMEM (1 mg/mL BSA, 10 mM HEPES). The plate was then serum starved in an incubator at 37 °C for approximately 16 hours (overnight) in the assaying medium.

Table 2. Transfection Conditions for pERK Assay.
Plus/minus each construct is marked with '+/-'. For Empty Vector, '+' represents 800 ng, '++' represents 1550 ng and '+++' represents 2300 ng.

DNA Construct	WT Cells	$\Delta G\alpha_{12/13}$ cells	$\Delta G\alpha_{12/13}$ cells + $G\alpha_{12}$	$\Delta G\alpha_{12/13}$ cells + $G\alpha_{13}$	$\Delta G\alpha_{12/13}$ cells + $G\alpha_{12}$ + $G\alpha_{13}$
Pplss-3HA-CB_1	+	+	+	+	+
NEV-Cytoplasmic	+	+	+	+	+
NEV-Nuclear	+	+	+	+	+
hGNA12	-	-	+	-	+
hGNA13	-	-	-	+	+
Empty Vector	+++	+++	++	++	+

pERK BRET1 assays were conducted in half plate reads (48 wells) in a LUMIstar® Omega plate reader, using 0.2 second detection per well. For each half plate read, cells were treated with 10 µL of Coelenterazine-h at 5 µM (Nanolight Technologies) and luminescence was detected simultaneously for a 5-minute pre-read at 37 °C to establish a stable baseline reading. THC, ZCZ and AMB were prepared to 10x final concentration from stock aliquots kept at -80 °C and diluted in drug vehicle containing assay medium, absolute ethanol (1:100) and DMSO (1:100). Following the pre-read, cells were stimulated with 10 µL of drug to make a final volume of 100 µL and were read for approximately 25 minutes. A set of wells were treated with 10 µL of phorbol-12-myristate-13-acetate at 10x final concentration (PMA, Cayman Chemical Company) to serve as a positive control for pERK stimulation. For both the pre-read and read, emissions at 475 nm (NLuc) and 535 nm (mVenus) were detected concurrently and recorded using the Omega Control software. BRET ratios (535/475 nm) were then exported using the Omega MARS software. GraphPad Prism v10 was used to graph and analyse data, producing kinetic time courses normalised to vehicle control, as well as concentration-response curves.

2.5 Internalisation and Cell Morphology

2.5.1 Receptor Trafficking Assay

In this research, immunocytochemistry was employed to assess receptor trafficking from the cell surface into the cytoplasm. Trafficking of receptors occurs after agonist stimulation, through the process of internalisation. This assay was carried out using a 'live-at-start' method, with primary antibody added prior to drug stimulation as previously described (Finlay et al., 2019). Receptor trafficking was arrested following drug stimulation, by placing the plate on an ice bed, and secondary antibody was added under non-permeabilising conditions. Thus, only receptor that was on the cell surface prior to drug addition will be labelled with secondary antibody, as it remains on the cell surface.

For each assay, the seeding, transfection, and plating of HEK293A WT and HEK 293A $\Delta G\alpha_{12/13}$ cells were performed as described above. Cells seeded onto 10 cm dishes were transfected with the relevant DNA constructs, depending on the condition:

- 1600 ng 3HA-hCB_1 pEF4A
- 50 ng untagged-hβ-arrestin-2 pcDNA3.1
- 350 or 400 ng Empty Vector pcDNA3.1 (to ensure a total DNA of 2 ng/dish)

Table 3 displays the transfection conditions used for 10 cm dishes in the assay, with cell line type and whether the condition had hGNA12 and/or hGNA13 added back to the $\Delta G\alpha_{12/13}$ cells. Following approximately 24 hours of incubation, cells were plated at a density of 2 x 10^4 cells per well on clear 96-well Costar® (Corning®) plates which were PDL-treated (~40 minutes to 1 hour).

Table 3. Transfection Conditions for Receptor Trafficking Assay.
Plus/minus each construct is marked with '+/-'. For Empty Vector, '+' represents 350 ng, '++' represents 400 ng.

DNA Construct	WT Cells + CB_1	$\Delta G\alpha_{12/13}$ cells + CB_1	WT cells + CB_1 + arrestin	$\Delta G\alpha_{12/13}$ cells + CB1 + arrestin
3HA-CB_1	+	+	+	+
hβ-Arrestin-2-Sp1	-	-	+	+
Empty Vector	++	++	+	+

Throughout the receptor trafficking protocol, the plates were kept at 37 °C during periods of incubation. Prior to adding primary antibody, plating media was aspirated and replaced with serum-free phenol red-free DMEM (1 mg/mL BSA). The plates were then serum starved for 30 minutes in the serum-free medium (SFM). SFM was aspirated and 35 µL/well primary mouse anti-HA antibody (BioLegend) was added (diluted 1:500 in SFM) and incubated for 30 minutes at 37 °C. Wells containing primary antibody were aspirated and washed twice with SFM prior to drug administration. THC (Toronto Research Chemicals Inc.) was diluted in SFM to the desired concentration and added for the appropriate time for the time-course trafficking (60, 30, 15, 8, 3, 0 minutes). All receptor trafficking conditions were designed to finish at the same time, with drugs aspirated from all wells and washed with SFM. This was followed by quickly moving the plate onto an ice bed to arrest the trafficking. (The drug administration step was carried out by Monica Patel for the trafficking protocol.)

For 30 mins at room temperature (RT), 35 µL secondary Alexa Fluor® 488 goat anti-mouse antibody (Thermo Fisher Scientific) was added (diluted 1:300 in SFM) to each well. Wells were washed twice with SFM, prior to fixing with 35 µL/well 4% paraformaldehyde (PFA, Thermo Fisher Scientific) for 10 minutes. Wells were twice-washed with PBS, followed by 35 µL/well Hoechst 33258 (Life Tech) diluted 1:500 in PBS containing 0.2% Triton-X100 (Sigma-Aldrich, PBS-T). Hoechst staining was incubated for 20 minutes at RT, followed by twice-washing with PBS-T. The plate was stored in PBS-T containing 0.4 mg/mL Merthiolate (Thermo Fisher Scientific, PBS-TM) at 4 °C in foil (light-protected) until imaging.

2.5.2 Assessment of Receptor Expression

Immunocytochemistry was used to assess differences in CB_1 expression in the different cell lines. Here, cell surface receptor and total receptor expression was examined. For each assay, the seeding, transfection. and plating of HEK293A WT and HEK 293A $\Delta G\alpha_{12/13}$ cells were

performed as described above. Cells seeded onto 6-well plates were transfected with the relevant DNA constructs scaled down from equivalent 10 cm dish values, depending on the condition:

- 276 ng pplss-3HA-hCB$_1$ pEF4A
- 130 ng hGNA12 and 130 ng hGNA13 pcDNA5
- 155 or 415 ng Empty Vector pcDNA3.1 (ensuring a total of 690 ng/well)

Table 4 displays the transfection conditions used for 6-well plates in the assay, with cell line type and whether the condition had hGNA12 and/or hGNA13 added back to the cells. Following approximately 24 hours of incubation, cells were plated at a density of 2.5 x 10^4 cells per well on clear 96-well Costar® (Corning®) plates which were PDL-treated (~40 minutes to 1 hour).

Table 4. Transfection Conditions for Assessment of Receptor Expression.
Plus/minus each construct is marked with '+/-'. For Empty Vector, the number of '+' indicates the amount added (approximately).

DNA Construct	WT Cells + CB_1	$\Delta G\alpha_{12/13}$ cells + CB_1	$\Delta G\alpha_{12/13}$ cells + $G\alpha_{12}$ + $G\alpha_{13}$ + CB_1
Pplss-3HA-CB_1	+	+	+
hGNA12	-	-	+
hGNA13	-	-	+
Empty Vector	++	++	+

After overnight incubation, plating media was then aspirated and washed with SFM. Then, 35 µL/well primary mouse anti-HA antibody (BioLegend, diluted 1:500 in SFM) was added to the cell surface receptor expression wells and incubated for 30 minutes at RT. Wells containing primary antibody were aspirated and washed with SFM, prior to fixing all cells (cell surface and total receptor expression wells). 35 µL/well 4% paraformaldehyde (PFA, Thermo Fisher Scientific) was added and incubated at RT for 10 minutes. Wells were thrice washed with PBS, before incubation of total receptor expression wells with 35 µL/well primary mouse anti-HA antibody (BioLegend, diluted 1:1000 in immuno-buffer) for 3 hours at RT or overnight at 4 °C.

Subsequently, all wells (cell surface and total receptor) were washed with PBS-T, prior to adding 35 µL/well secondary Alexa Fluor® 488 goat anti-mouse antibody (Thermo Fisher Scientific, diluted 1:400 in immuno-buffer) incubated for 3 hours at RT or overnight at 4 °C. Secondary antibody was removed from all wells and washed with PBS-T, prior to 35 µL/well Hoechst 33258 (Life Tech) diluted 1:500 in PBS-T. Hoechst staining was incubated for 20 minutes at RT, followed by washing with PBS-T. The plate was stored in PBS-TM at 4 °C in foil (light-protected).

2.5.3 Assessment of Cell Morphology Changes

Immunocytochemistry was also used to assess differences in cellular morphology in the different cell lines. The seeding, transfection, and plating of HEK293A WT and HEK 293A $\Delta G\alpha_{12/13}$ cells were performed as described above. Cells seeded onto 6-well plates were transfected with the relevant DNA constructs scaled down from equivalent 10 cm dish values, depending on the condition:

- 130 ng hGNA12 and 130 ng hGNA13 pcDNA5
- 430 or 690 ng Empty Vector pcDNA3.1 (ensuring a total of 690 ng/well)

Table 5. Transfection Conditions for Assessment of Cellular Morphology Changes.
Plus/minus each construct is marked with '+/-'. For Empty Vector, the number of '+' indicates the amount added (approximately).

DNA Construct	WT Cells	$\Delta G\alpha_{12/13}$ cells	$\Delta G\alpha_{12/13}$ cells + $G\alpha_{12}$ + $G\alpha_{13}$
hGNA12	-	-	+
hGNA13	-	-	+
Empty Vector	+++	+++	++

Table 5 displays the transfection conditions used for 6-well plates in the assay, with cell line type and whether the condition had hGNA12 and/or hGNA13 added back to the cells. Following approximately 24 hours of incubation, cells were plated at a density of 2.5 x 10^4 cells per well on clear 96-well Costar® (Corning®) plates which were PDL-treated (~40 minutes to 1 hour).

After overnight incubation, plating media was then aspirated and washed with SFM. 35 µL/well 4% paraformaldehyde (PFA, Thermo Fisher Scientific) was added and incubated at RT for 10 minutes. Wells were thrice washed with PBS, before staining with Phalloidin iFluor-488 for 60 minutes (Abcam, diluted 1:1000 in PBS + 1% BSA). Phalloidin was removed from all wells and washed with PBS, prior to 35 µL/well Hoechst 33258 (Life Tech) diluted 1:500 in PBS-T. Hoechst staining was incubated for 20 minutes at RT, followed by washing with PBS-T. The plate was stored in PBS-TM at 4 °C in foil (light-protected).

2.5.4 Imaging and Analysis

For both receptor trafficking and assessment of cell morphology, imaging was conducted using an Opera Phenix® microscope. Images were collected using the 10x or 20x objective lens at 4 or 24 sites per well, depending on the experiment and analysed in the Signals Image Artist software. Receptor and nuclear staining were measured by collecting emission data from Alexa Fluor® 488 (excitation 488 nm, emissions at 500-550 nm) and Hoechst 33258 (excitation 405 nm, emissions at 435-480 nm). For receptor internalisation, Signals Image Artist was used to analyse the images to measure the number of nuclei and intensity of Alexa Fluor® 488 fluorescence. Intensity per well was divided by the number of nuclei to produce an average integrated intensity per cell. Data was then plotted in GraphPad PRISM v10 and fitted with a one-phase exponential decay model. (The imaging and staining quantification was carried out by Monica Patel, as there was insufficient time for training to use the high-power microscope).

2.6 Data and Statistical Analysis

The data in BRET assays was generated as raw BRET counts using a LUMIStar Omega (BMG Labtech GmbH) and expressed as a BRET ratio, automatically calculated in the Omega MARS Software. BRET ratios were graphed in GraphPad PRISM v10 and were baseline corrected to vehicle values (or lowest drug concentration if necessary). Baseline corrected values were analysed using an area under the curve analysis, which were then presented as sigmoidal concentration-response curves. Curves were generated in GraphPad PRISM v10 using a three parameter, non-linear regression curve fit. Concentration response data displayed are representative from a single experiment (expressed as mean ± SD) to avoid distortion of the slope (Hall & Langmead, 2010). Where possible, time course data are presented as combined averages expressed as mean ± SEM of *n* biological replicates, or a representative repeat if averaging was not possible (*n* indicated in respective legends). A biological replicate

constituted the experiment being repeated with the drugs prepared separately on a different passage of cells. Each biological replicate had three technical replicates per drug/vehicle condition. Statistical analyses were carried out using a one-way ANOVA or unpaired t-test where appropriate, with a Holm-Šídák post-hoc test carried out where a significant ANOVA ($p < 0.05$) was reported.

3 Results

3.1 $G\alpha_{12/13}$ Dissociation at CB_1

The ability of CB_1 to activate $G\alpha_{12/13}$ proteins in HEK293A wild type (WT) cells was assessed using the TRUPATH G protein dissociation BRET2 assay (as described in Methods 2.2). The BRET ratio (515/410 nm) was recorded for 0.5 seconds for every well consecutively for a 20-minute period and is equated to the amount of G protein dissociation. In this assay, three structurally distinct agonists were employed to assess the effect of each ligand on $G\alpha_{12/13}$ activation at a range of concentrations: THC, AMB and ZCZ.

Figure 5 presents the vehicle-subtracted averaged BRET ratio for G protein dissociation of $G\alpha_{12}$ (Fig. 5A) and $G\alpha_{13}$ proteins (Fig. 5B) (n = 5). Each time course compares the G protein dissociation of CB_1 agonists THC, AMB and ZCZ at a single, high concentration, based on the efficacy and potency of these drugs in other G protein dissociation assays. THC (31.6 µM) appeared to produce only a small change in $G\alpha_{12}$ dissociation (Fig. 5A) and little-to-no effect on $G\alpha_{13}$ dissociation (Fig. 5B). However, both AMB (1 µM) and ZCZ (10 µM) were able to

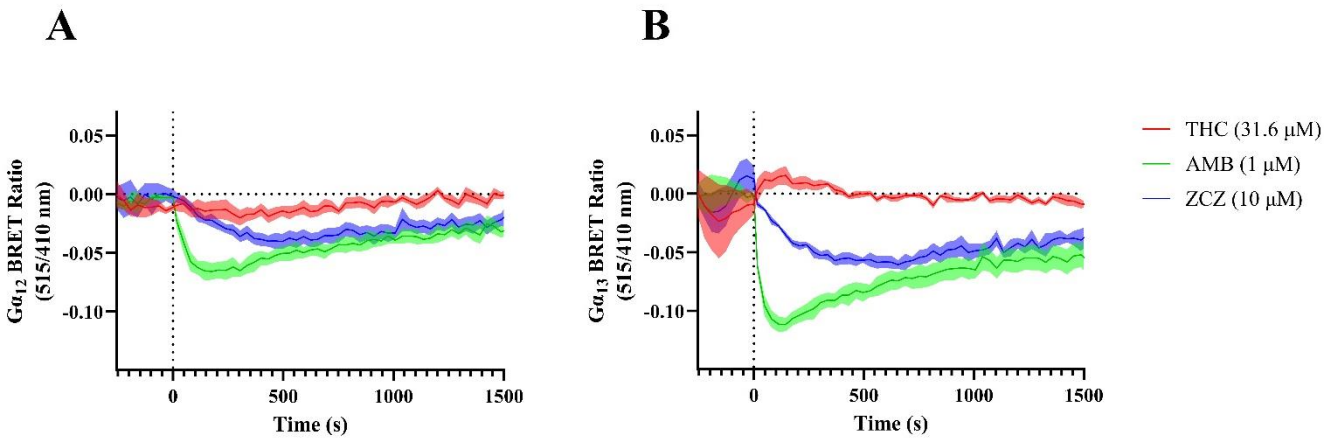

Figure 5. Kinetic BRET time-course data for $G\alpha_{12/13}$ protein dissociation at CB_1.
HEK293A wild type cells were transfected with CB_1 and dissociation of either $G\alpha_{12}$ **(A)** or $G\alpha_{13}$ **(B)** was measured with the TRUPATH assay. Cells were stimulated for 20 minutes with agonists THC (31.6 µM), AMB-FUBINACA (AMB, 1 µM) or ZCZ-011 (ZCZ, 10 µM). Data is presented as vehicle-subtracted mean ± SEM from 5 biologically independent experiments, carried out in triplicate within each assay.

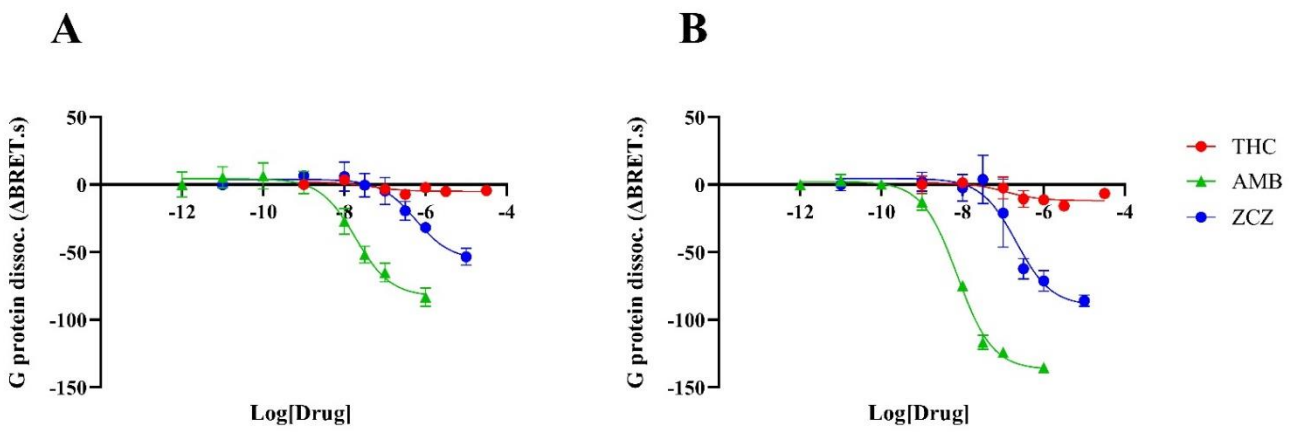

Figure 6. Concentration response curves for Gα12/13 protein dissociation at CB1. HEK293A wild type cells were transfected with CB_1 and dissociation of either $G\alpha_{12}$ **(A)** or $G\alpha_{13}$ **(B)** was measured with the TRUPATH assay. Cells were serum starved for ≥ 30 minutes prior assaying. Cells were stimulated for 20 minutes at a range of concentrations with agonists THC, AMB-FUBINACA (AMB) or ZCZ-011 (ZCZ). Kinetic traces were analysed by AUC at each concentration to generate concentration response curves. Representative data is presented as mean ± SD of data collected in triplicate from one of five independent biological replicates.

cause $G\alpha_{12/13}$ dissociation. AMB seemed to display more rapid G protein dissociation initially (especially in activating $G\alpha_{13}$), though lowered to levels only slightly greater than ZCZ around 500 seconds into the assay.

After initial assessment, time course BRET ratios were further analysed using area under the curve (AUC) calculations. The AUC data was then fitted as non-linear concentration-response curves with a three-parameter regression curve fit, which are displayed in Figure 6. Both AMB and ZCZ display a concentration-dependent increase in activation of $G\alpha_{12}$ (Fig. 6A) and $G\alpha_{13}$ (Fig. 6B) proteins. Due to the small response window, THC appears to not show a clear concentration-dependent response in $G\alpha_{12}$ dissociation and very slightly in $G\alpha_{13}$ dissociation. Through the non-linear curve fit, potencies can be attained as pEC_{50} values and efficacies as E_{MAX} (span) values (Table 6). There was a sizeable difference in potency between ligands in $G\alpha_{12}$ dissociation, with AMB being the most potent at 12.0 nM (pEC_{50} 7.92 ± 0.08) (Table 6). THC was less potent at 58.9 nM (pEC_{50} 7.23 ± 0.30), and ZCZ even less so at 389 nM (pEC_{50}

6.41 ± 0.05). There was a similar trend in potencies for $G\alpha_{13}$ dissociation; AMB was the most potent at 12.0 nM (pEC_{50} 7.92 ± 0.08), THC was less potent at 70.8 nM (pEC_{50} 7.15 ± 0.27) and ZCZ was least potent at 363 nM (pEC_{50} 6.44 ± 0.13) (Table 6). Using one-way ANOVA testing with Holm-Šídák post-hoc comparisons, there was no significant difference in potency for any ligand between G proteins. For both $G\alpha_{12}$ and $G\alpha_{13}$ dissociation AMB displayed the highest efficacy, then ZCZ and THC with the lowest (Fig. 6; Table 6). However, upon further investigation, the E_{MAX} of THC for $G\alpha_{12}$ and $G\alpha_{13}$ proteins was not significantly different from zero. Analysis revealed no difference between efficacies between G proteins for THC or ZCZ, but the efficacy of AMB was lower in $G\alpha_{12}$ dissociation, than in $G\alpha_{13}$ dissociation (Table 6).

Table 6. Efficacies and potencies of CB_1 agonists for $G\alpha_{12/13}$ dissociation.

	$G\alpha_{12}$			$G\alpha_{13}$		
	pEC_{50} (M)	E_{MAX} (ΔBRET.s)	*n*	pEC_{50} (M)	E_{MAX} (ΔBRET.s)	*n*
AMB-FUBINACA	7.92 (0.08)	73.01 (7.45)	5	7.92 (0.08)	117.7 (9.52)	5
THC	7.23 (0.30)	17.17 (4.54)	5	7.15 (0.27)	12.95 (1.57)	4
ZCZ-011	6.41 (0.05)	53.98 (7.82)	5	6.44 (0.13)	79.85 (9.42)	5

Each individual concentration response curve was carried out in triplicate and fitted with the three parameter E_{MAX} model to find E_{MAX} (span) and pEC_{50}, with data presented as mean (± SEM) from *n* independent biological replicates. Experimental groups are HEK293A Wild Type cells transfected with CB_1 and either $G\alpha_{12}$ or $G\alpha_{13}$ proteins.

3.2 β-arrestin Translocation

The effect of $G\alpha_{12/13}$ proteins on β-arrestin 2 recruitment was assessed using the β-arrestin translocation BRET1 assay (as described in Methods 2.3). The BRET ratio (535/475 nm) was recorded for 0.35 seconds for every well consecutively for a 20-minute period and is equated to the level of β-arrestin recruitment. In this assay, THC and ZCZ were tested at the same concentration as they were in the G protein dissociation assay, whilst AMB was tested over a

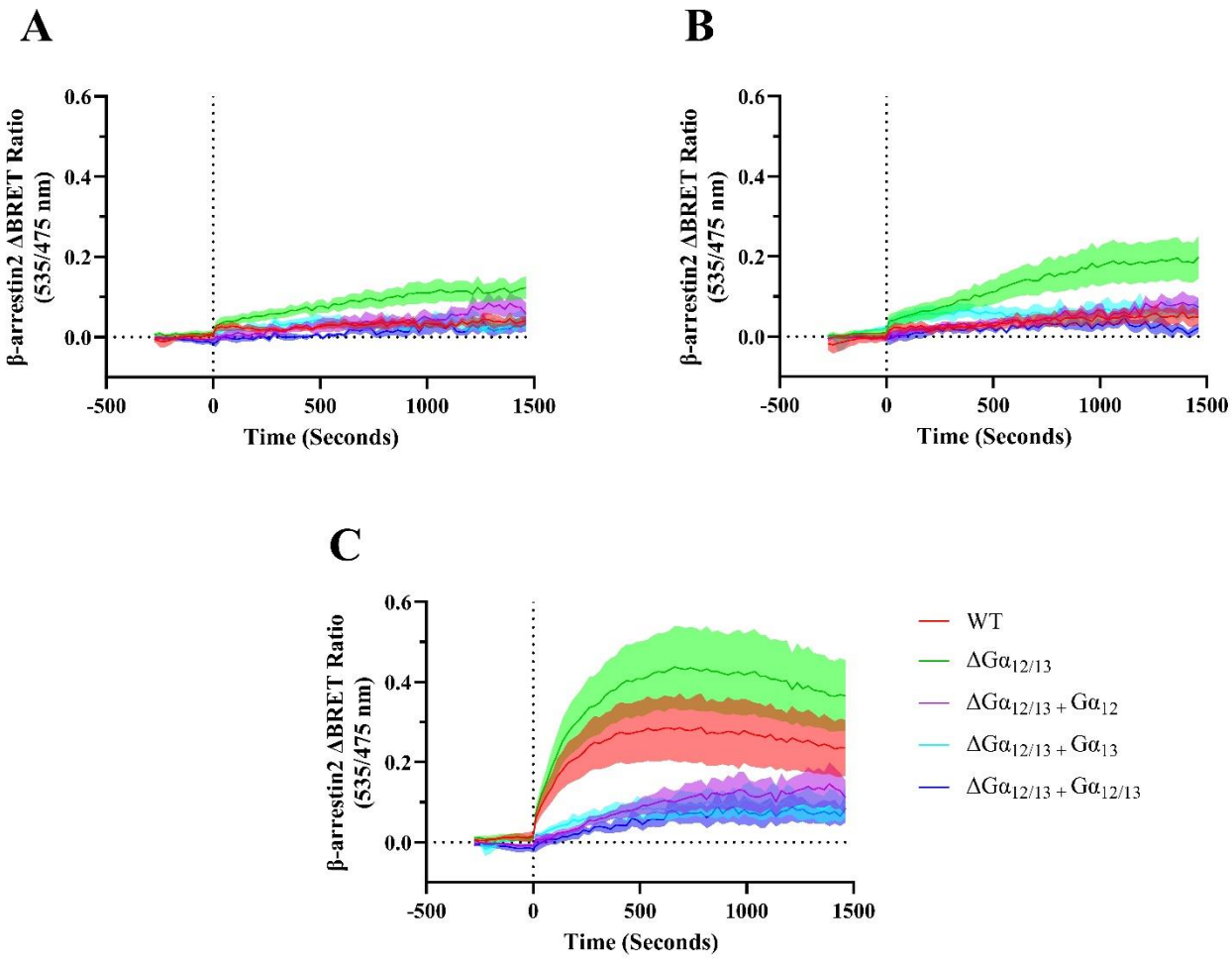

Figure 7. Kinetic BRET time-course for β-arrestin translocation at CB_1.
HEK293A wild type (WT) cells and $G\alpha_{12/13}$ knock-out ($\Delta G\alpha_{12/13}$) cells were transfected with β-arrestin translocation constructs and CB_1. Additionally, HEK293A $\Delta G\alpha_{12/13}$ cells were transfected with $G\alpha_{12/13}$ proteins individually and together. Cells were serum starved for ≥ 30 minutes prior assaying, with cells were stimulated for 20 minutes with agonist. **A)** THC (10 μM), **B)** ZCZ-011 (10 μM). **C)** AMB-FUBINACA (1 μM). Data is presented as vehicle-subtracted mean ± SEM from 5 biologically independent experiments, carried out in triplicate within each assay.

range of concentrations to produce a concentration-response curve, due to having more robust signal size.

Figure 7 presents the vehicle-subtracted averaged time course BRET ratios for β-arrestin translocation, for the three agonists used (THC, ZCZ, AMB) ($n = 5$). Each time course compares β-arrestin translocation in the following cell lines: HEK293A wild type (WT), HEK293A knock-out $G\alpha_{12/13}$ ($\Delta G\alpha_{12/13}$) and $\Delta G\alpha_{12/13}$ cells with $G\alpha_{12}$ or $G\alpha_{13}$ transfected individually and together. When stimulated with THC (10 µM) (Fig. 7A), ZCZ (10 µM) (Fig. 7B) or AMB (1 µM) the $\Delta G\alpha_{12/13}$ cells alone produced an increase in β-arrestin translocation compared to the WT cells. The addition of $G\alpha_{12}$ and $G\alpha_{13}$ individually or together reduced agonist-dependent β-arrestin translocation in $\Delta G\alpha_{12/13}$ cells to almost zero (Fig. 7A, 7B, 7C). In the cells transfected

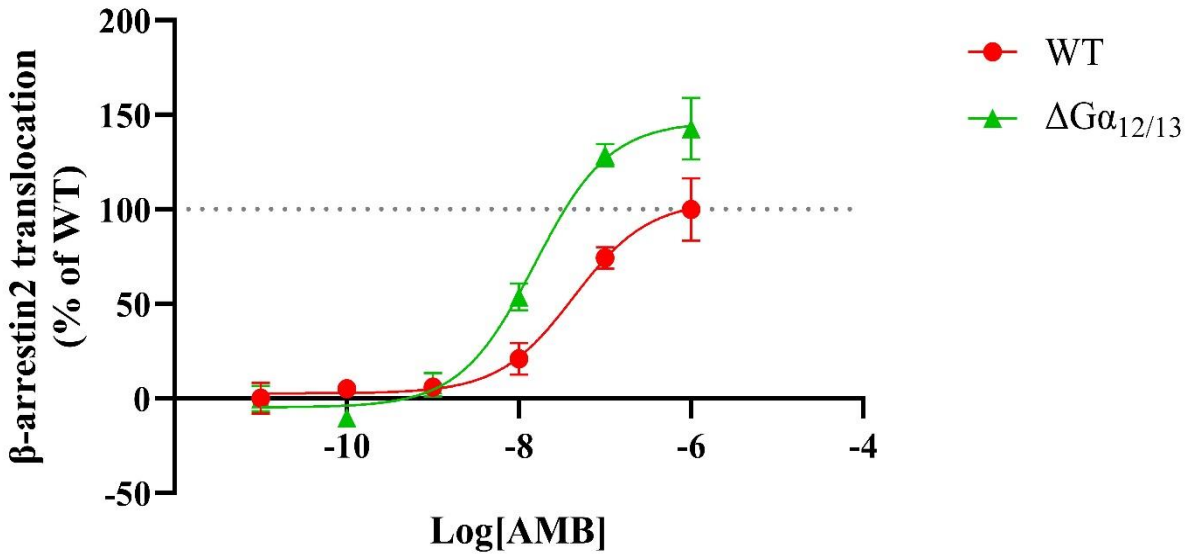

Figure 8. Concentration response curves for β-arrestin Translocation at CB_1.
HEK293A wild type (WT) cells and $G\alpha_{12/13}$ knock-out ($\Delta G\alpha_{12/13}$) cells were transfected with β-arrestin translocation constructs and CB_1. Cells were serum starved for ≥ 30 minutes prior assaying. Cells were stimulated for 20 minutes at a range of concentrations with AMB-FUBINACA (AMB). Kinetic traces were analysed by AUC at each concentration to generate concentration response curves, and then individual curves were normalised to the maximum response in WT cells. Representative data is presented as mean ± SD of data collected in triplicate from one of five independent biological replicates.

with exogenous $G\alpha_{12/13}$, β-arrestin translocation was pushed lower than it was in WT cells stimulated with AMB, though not completely removed (Fig. 7C).

Time course data for AMB-mediated β-arrestin translocation was analysed using area under the curve analysis (AUC) to generate a concentration-response curve. A three parameter, non-linear model of regression was used to generate the data presented in Figure 8. Here, the amount of AMB-induced β-arrestin translocation was normalised to WT levels for each assay, revealing the $\Delta G\alpha_{12/13}$ condition to be substantially increased over WT (Fig. 8). Through the non-linear curve fit for each biological replicate, potencies were obtained as pEC_{50} values and efficacies as E_{MAX} (span) values (Table 7). There was no statistically significant difference in potency between WT (20.9 nM, pEC_{50} 7.68 ± 0.12) and $\Delta G\alpha_{12/13}$ conditions (18.6 nM, pEC_{50} 7.73 ± 0.04) (unpaired t-test, $p = 0.7078$) (Table 7). However, there was a significant difference in the efficacy between the groups for non-normalised data (unpaired t-test, $p = 0.0367$) (Table 7). The $\Delta G\alpha_{12/13}$ group was more efficacious for β-arrestin translocation (E_{MAX} 117.7 ± 9.52), and the WT group was lower in efficacy (E_{MAX} 73.01 ± 7.45) (Table 7).

Table 7. Efficacies and potencies of β-arrestin translocation at CB_1 in HEK293A WT and $\Delta G\alpha_{12/13}$ cells.

	WT			$\Delta G\alpha_{12/13}$		
	pEC_{50} (M)	E_{MAX} (ΔBRET.s)	*n*	pEC_{50} (M)	E_{MAX} (ΔBRET.s)	*n*
AMB-FUBINACA	7.68 (0.12)	73.01 (7.45)	5	7.73 (0.04)	117.7* (9.52)	5

Each individual concentration response curve was carried out in triplicate and fitted with the three parameter E_{MAX} model to find E_{MAX} (span) and pEC_{50}, with data presented as mean (± SEM). Experimental groups are HEK293A Wild Type (WT) and $G\alpha_{12/13}$ protein knock-out ($\Delta G\alpha_{12/13}$) cell lines, stimulated with AMB-FUBINACA at a range of concentrations. Statistically significant differences in E_{MAX}/pEC_{50} were assessed using unpaired t-tests ($p < 0.05$), analysed in GraphPad PRISM. *n* represents the number of independent biological replicates, with technical replicates carried out in triplicate.
* Indicates a significant increase ($p = 0.0367$) in E_{MAX}, comparing between WT and $\Delta G\alpha_{12/13}$. No statistically significant difference was detected between pEC_{50} values ($p = 0.7078$).

3.3 ERK Phosphorylation

The effect of $G\alpha_{12/13}$ proteins and enhanced β-arrestin recruitment on ERK phosphorylation was assessed using the pERK BRET1 assay (as described in Methods 2.4). The BRET ratio (535/475 nm) was recorded for 0.2 seconds for every well consecutively for a 20-minute period and is proportional to the amount of ERK phosphorylation. In this assay, THC and ZCZ were tested at the maximal concentration from the previous assays, with AMB tested at a range of concentrations.

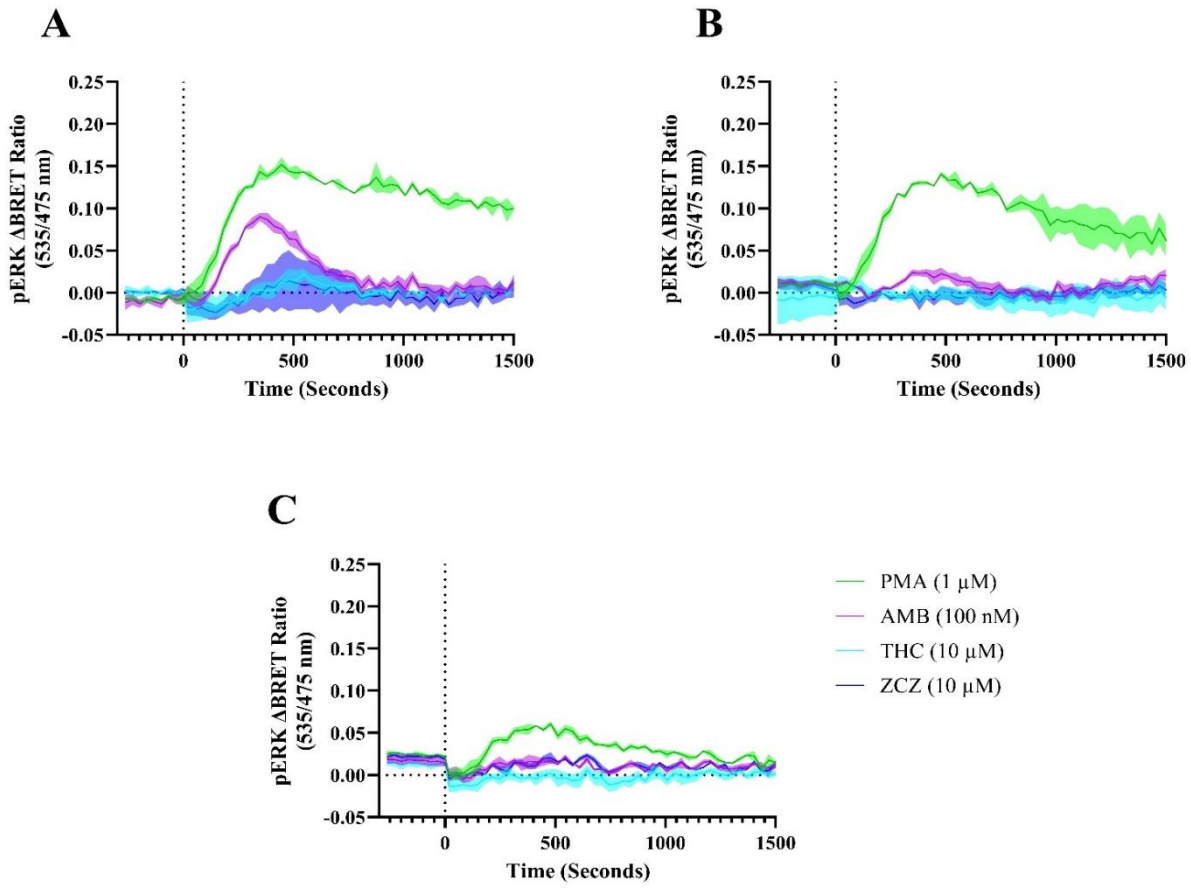

Figure 9. Kinetic BRET time-course for ERK phosphorylation at CB_1.
HEK293A wild type (WT; **A**) cells and $G\alpha_{12/13}$ knock-out ($\Delta G\alpha_{12/13}$; **B**) cells were transfected with pERK BRET constructs and CB_1. Additionally, HEK293A $\Delta G\alpha_{12/13}$ cells were transfected with $G\alpha_{12/13}$ **(C)**. Cells were serum starved for ≥ 30 minutes prior assaying. Cells were stimulated for 20 minutes with agonists THC (10 μM), AMB-FUBINACA (AMB, 100 nM) or ZCZ-011 (ZCZ, 10 μM). PMA (1 μM) served as a positive control in this experiment. Representative data is presented as mean ± SEM of data collected in triplicate from one of five independent biological replicates.

Figure 9 presents a representative vehicle-subtracted time course of BRET ratios for ERK phosphorylation, for the three agonists used (THC, ZCZ, AMB) at their maximum concentration. As the distribution of data points was randomised between plate maps, the data could not be combined between experiments (n = 4-5), due to different time points being collected. Each time course compares the ERK phosphorylation of CB_1 agonists THC, AMB and ZCZ at the maximal concentrations used in this assay. In these assays, phorbol-12-myristate-13-acetate (Cayman, PMA, 1 µM), served as a positive control for ERK phosphorylation (Fig. 9 green traces). In the HEK293A wild type (WT) cells, AMB (100 nM) produced the highest peak in ERK phosphorylation. This was followed by ZCZ (10 µM) and THC (10 µM) with roughly equal peaks, although there was a lot of variation in the ZCZ ERK phosphorylation (Fig. 9A). WT ERK phosphorylation traces across all the agonists exhibited a transient signal, returning to zero at approximately 16 minutes (1000 seconds) into the stimulation period. Interestingly, the HEK293A knock-out $G\alpha_{12/13}$ ($\Delta G\alpha_{12/13}$) cells exhibited

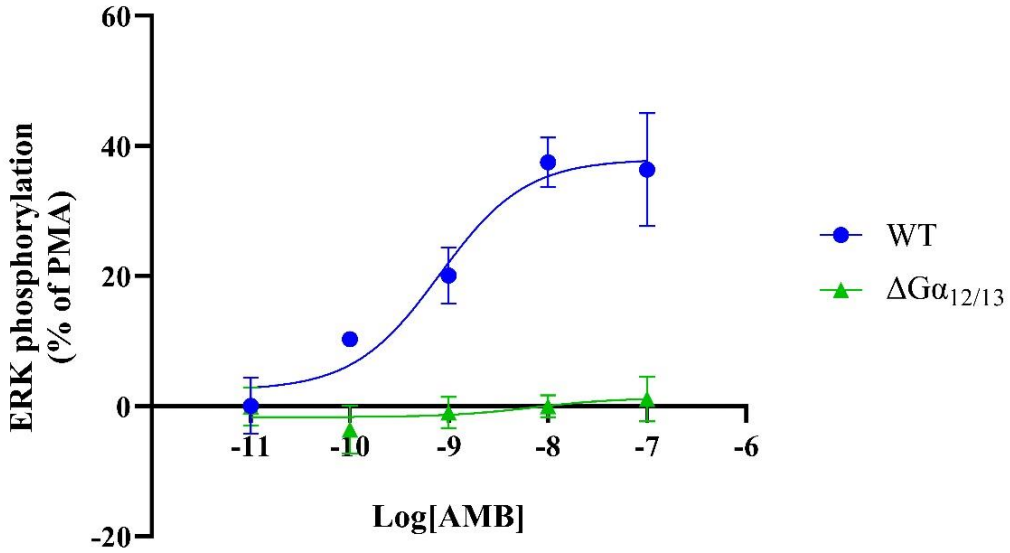

Figure 10. Concentration response curves for ERK phosphorylation at CB_1.
HEK293A wild type (WT) cells and $G\alpha_{12/13}$ knock-out ($\Delta G\alpha_{12/13}$) cells were transfected with ERK phosphorylation constructs and CB_1. Cells were serum starved for ≥ 30 minutes prior assaying. Cells were stimulated for 20 minutes at a range of concentrations with AMB-FUBINACA (AMB). Kinetic traces were analysed by AUC to generate concentration response data and then normalised to PMA stimulation of ERK. Representative data is presented as mean ± SD of data collected in triplicate from one of five independent biological replicates.

almost zero increase in phosphorylation of ERK across any of the ligands tested despite a similar PMA response (Fig. 9B). The addition of $G\alpha_{12/13}$ proteins to the $\Delta G\alpha_{12/13}$ cells failed to restore the ERK phosphorylation levels back to those seen in WT (Fig. 9C). In addition, the PMA signal in the $\Delta G\alpha_{12/13}$ cells with $G\alpha_{12/13}$ added was markedly lower than in the other conditions (Fig. 9).

Following initial assessment, time course ERK phosphorylation BRET ratios for AMB were further analysed using area under the curve (AUC) calculations. The AUC data was then fitted as non-linear concentration-response curves with a three-parameter regression curve fit, which are displayed in Figure 10. Here, the amount of AMB-induced ERK phosphorylation was normalised to PMA levels, revealing the WT condition to show a significant increase over $\Delta G\alpha_{12/13}$ condition, which had almost no response (Fig. 10). Through the non-linear curve fit, potencies were obtained as pEC_{50} values and efficacies as E_{MAX} (span) values for the WT condition (Table 8). As the $\Delta G\alpha_{12/13}$ cells showed almost no response, pEC_{50} and E_{MAX} was not measurable. AMB induced ERK phosphorylation in WT cells with an E_{MAX} of 30.74 ± 5.62 and a pEC_{50} of 1.44 nM (8.84 ± 0.16) (Table 8).

Table 8. Efficacies and potencies of the effect of $\Delta G\alpha_{12/13}$ on ERK phosphorylation at CB_1.

	WT			$\Delta G\alpha_{12/13}$		
	pEC_{50} (M)	E_{MAX} (ΔBRET.s)	*n*	pEC_{50} (M)	E_{MAX} (ΔBRET.s)	*n*
AMB-FUBINACA	8.84 (0.16)	30.74 (5.62)	4	Not Measurable	Not Measurable	5

Each individual concentration response curve was carried out in triplicate and fitted with the three parameter E_{MAX} model to find E_{MAX} (span) and pEC_{50}, with data presented as mean (± SEM). Experimental groups are HEK293A Wild Type (WT) and $G\alpha_{12/13}$ protein knock-out ($\Delta G\alpha_{12/13}$) cell lines, stimulated with AMB-FUBINACA at a range of concentrations.
n represents the number of independent biological replicates, with each experimental replicate carried out in triplicate.

3.4 Receptor Trafficking, Expression and Morphological Changes

The effect of $G\alpha_{12/13}$ proteins and enhanced β-arrestin recruitment on CB_1 internalisation was assessed using a receptor trafficking assay (as described in Methods 2.5.1). The level of cell surface CB_1 expression was measured using immunocytochemistry for a range of drug stimulation time points over a 60-minute period (0, 3, 8, 15, 30 and 60 minutes). To induce receptor trafficking, THC was used at the maximal concentration from β-arrestin translocation assays (10 µM) and at an approximate EC_{50} concentration (31.6 nM).

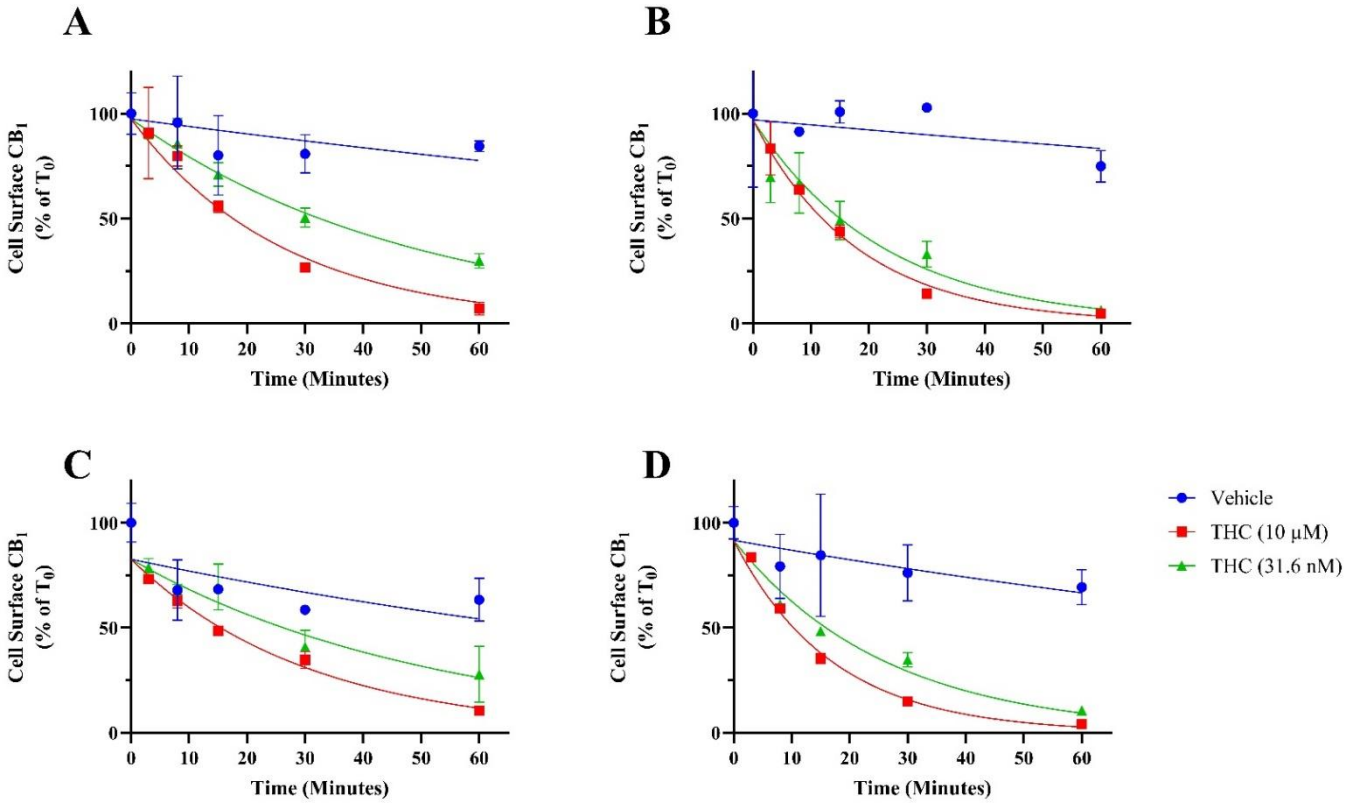

Figure 11. Receptor Trafficking of CB_1.
HEK293A wild type (WT) cells and $G\alpha_{12/13}$ knock-out ($\Delta G\alpha_{12/13}$) cells were transfected with CB_1. Additionally, some cells were transfected with β-arrestin-2. **A)** WT cells, **B)** WT cells with β-arrestin-2, **C)** $\Delta G\alpha_{12/13}$ cells, **D)** $\Delta G\alpha_{12/13}$ cells with β-arrestin-2. Cells were serum starved for ≥ 30 minutes prior assaying. Cells were stimulated for 0, 3, 8, 15, 30 or 60 minutes with two of concentrations of THC (10 µM and 31.6 nM). Data is presented as mean ± SD, normalized to vehicle time-zero (T_0) for a single experiment performed in triplicate.

Figure 11 presents the non-linear one-phase decay curves of cell surface CB_1 expression normalised to time zero (T_0) expression, in HEK293A wild type (WT) and HEK293A knock-out $G\alpha_{12/13}$ ($\Delta G\alpha_{12/13}$) cells. Here, receptor trafficking assays were conducted in each of the cell lines with and without transfection of additional β-arrestin 2. Between WT cells and $\Delta G\alpha_{12/13}$ cells, there was no clear difference in internalisation kinetics at either concentration of THC (Fig. 11A vs 11C, Fig. 11B vs 11D). However, the addition of β-arrestin appeared to speed up the internalisation of CB_1 compared to no β-arrestin, in both WT (Fig. 11A vs 11B) and $\Delta G\alpha_{12/13}$ cells (Fig. 11C vs 11D). This was also confirmed through the assessment of CB_1 internalisation half-lives in each cell line at two concentrations of THC (Table 9), via analysis of the non-linear one-phase decay curves. Interestingly, in the non-normalised raw traces (not shown), the initial cell surface CB_1 levels appeared to be higher in the $\Delta G\alpha_{12/13}$ cells than in the WT cells. Due to time constraints this experiment was only repeated once.

Table 9. CB_1 Internalisation Half-lives in HEK293A cells.

	Condition	Half-life (minutes)
THC (10 μM)	WT	18.25
	WT + β-arrestin	12.48
	$\Delta G\alpha_{12/13}$	21.26
	$\Delta G\alpha_{12/13}$ + β-arrestin	11.80
THC (31.6 nM)	WT	33.75
	WT + β-arrestin	15.71
	$\Delta G\alpha_{12/13}$	36.19
	$\Delta G\alpha_{12/13}$ + β-arrestin	18.18

Each individual internalisation curve was carried out in triplicate and fitted with the one-phase decay curve fit to find half-life. Experimental groups are HEK293A Wild Type (WT) and $G\alpha_{12/13}$ protein knock-out ($\Delta G\alpha_{12/13}$) cell lines transfected with CB_1 and β-arrestin (depending on condition), stimulated with THC at 10 μM and 31.6 nM. Data presented from one biological repeat.

After measuring CB_1 trafficking, receptor expression was assessed to determine if it varied between WT cells, $\Delta G\alpha_{12/13}$ cells and $\Delta G\alpha_{12/13}$ cells with $G\alpha_{12/13}$ proteins reintroduced. Here, CB_1 was fluorescently labelled, and nuclei were stained using immunocytochemistry techniques, prior to being imaged (as described in Methods 2.5.2 and 2.5.4) (Figure 12). Furthermore, cell surface and total CB_1 expression was quantified through analysing the level

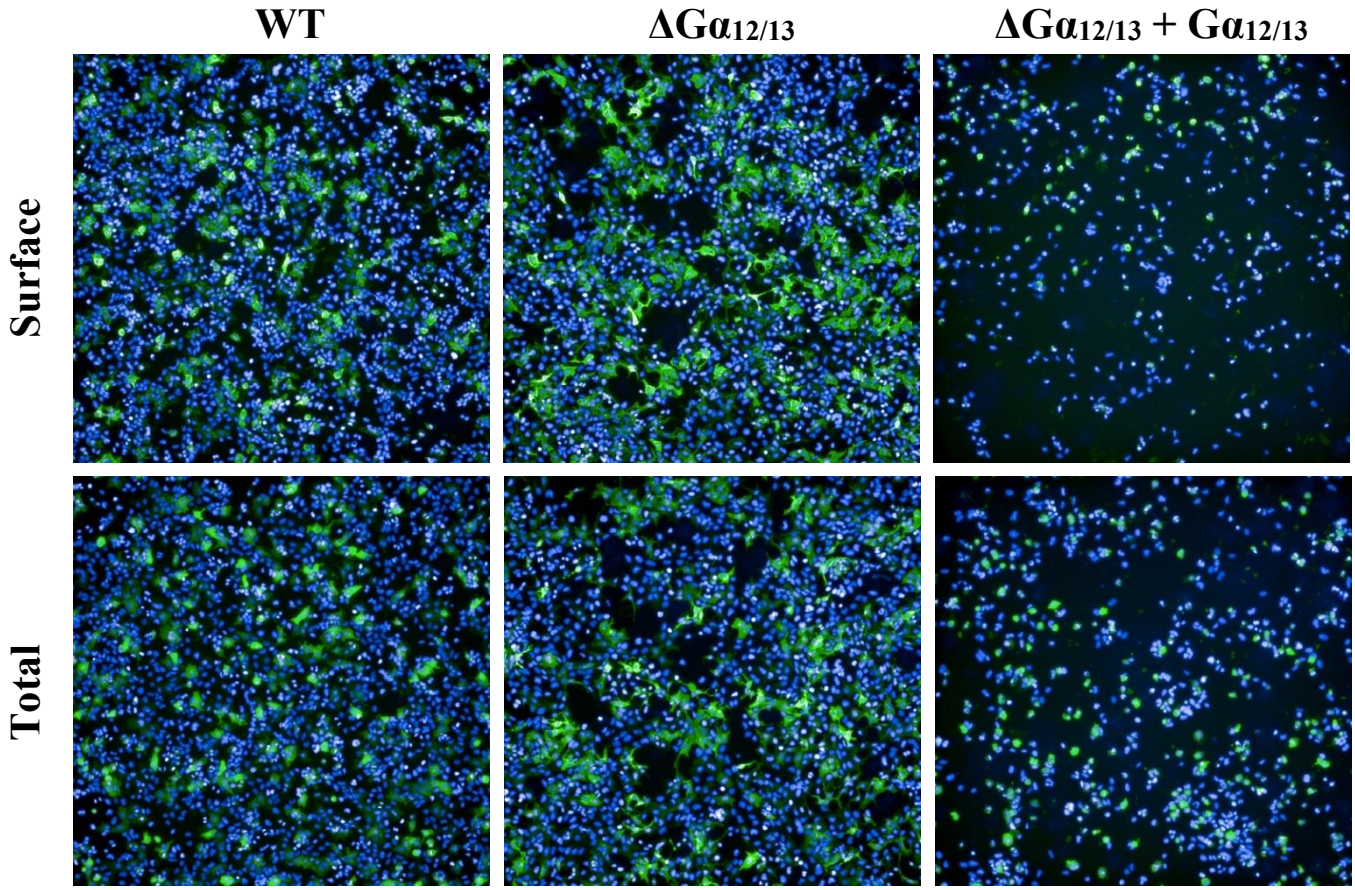

Figure 12. Receptor Expression Images for CB_1 in HEK293A Wild Type and $\Delta G\alpha_{12/13}$ cells.
Immunocytochemistry images of HEK293A wild type (WT) and knock-out $G\alpha_{12/13}$ ($\Delta G\alpha_{12/13}$) cells with CB_1 transfected. Additionally, $\Delta G\alpha_{12/13}$ cells were transfected with $G\alpha_{12/13}$ proteins. Distribution of HA-tagged CB_1 was assessed using primary mouse anti-HA and secondary Alexa Fluor 488 goat anti-mouse staining (green). Hoechst 33258 staining (blue) highlights nuclei. Images present the surface level of CB_1 expression (top row) and level of total receptor staining (bottom row), between cell lines. Images shown were taken with the 10x-objective lens from 4 sites per well. Images are representative of three experimental replicates from one biological replicate.

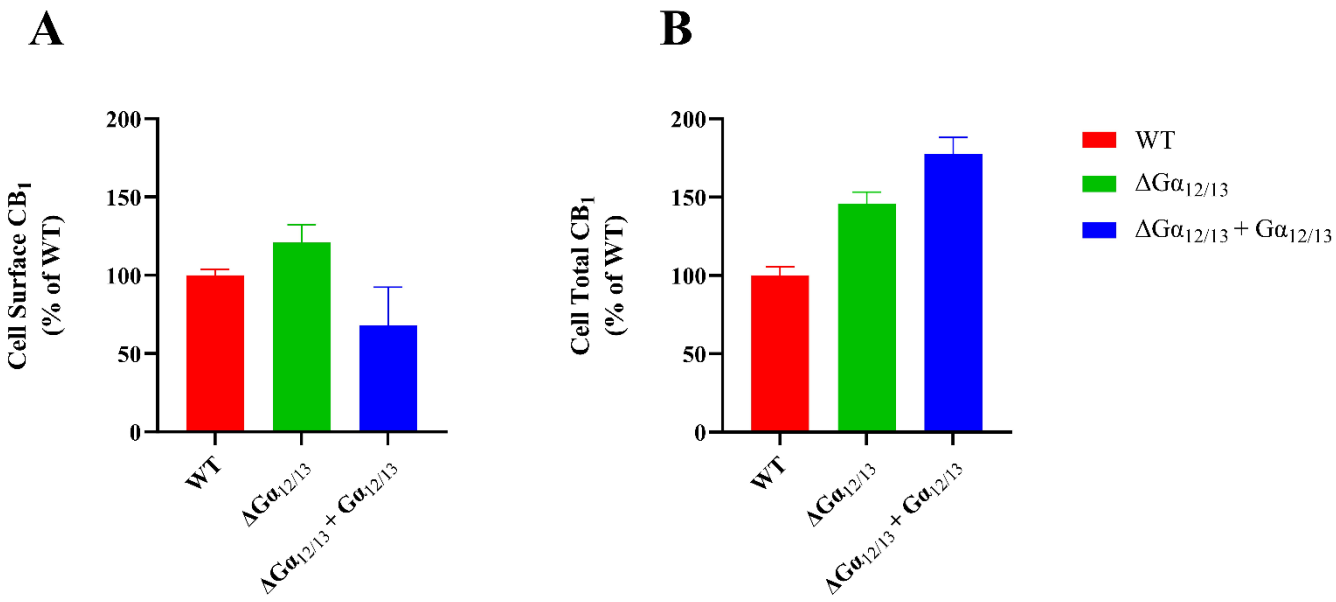

Figure 13. Receptor Expression Quantification for CB_1 in HEK293A Wild Type and $\Delta G\alpha_{12/13}$ cells.
Cell surface and total receptor expression was quantified from immunocytochemistry images of HEK293A wild type (WT) and knock-out $G\alpha_{12/13}$ ($\Delta G\alpha_{12/13}$) cells, as seen in Figure 12 above. Receptor expression was quantified using the amount of fluorescence produced by Alexa Fluor 488 and the number of nuclei present to give an average integrated intensity per well. Data is normalized to WT expression and is displayed as mean ± SD, from one experimental replicate carried out in triplicate (n = 1).

of fluorescence produced and then normalised to WT CB_1 expression (Figure 13). The $\Delta G\alpha_{12/13}$ cells displayed approximately 20% more cell surface CB_1 expression than WT cells (Fig. 12, Fig. 13A). The addition of $G\alpha_{12/13}$ protein back into the $\Delta G\alpha_{12/13}$ cells lowered the cell surface expression to around 30% below WT expression (Fig. 12, Fig. 13A). Total CB_1 expression was also evaluated, which showed $\Delta G\alpha_{12/13}$ cells displayed nearly 50% more CB_1 expression than WT cells (Fig. 12, Fig. 13B). Interestingly, $\Delta G\alpha_{12/13}$ cells with $G\alpha_{12/13}$ proteins transfected showed nearly 80% more total CB_1 expression than WT cells (Fig. 12, Fig. 13B).

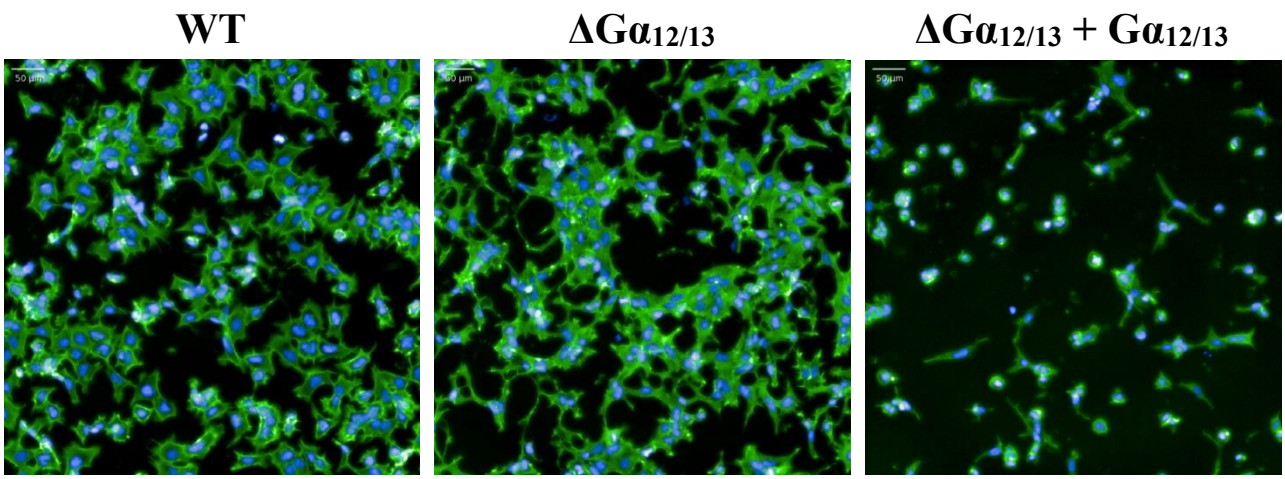

Figure 14. Phalloidin Staining for Actin Cytoskeleton in HEK293A Wild Type and $\Delta G\alpha_{12/13}$ cells.
Immunocytochemistry images of HEK293A wild type (WT) and knock-out $G\alpha_{12/13}$ ($\Delta G\alpha_{12/13}$) cells. Additionally, $\Delta G\alpha_{12/13}$ cells were transfected with $G\alpha_{12/13}$ proteins. Phalloidin iFluor-488 staining (green) reveals the actin cytoskeleton distribution within cells, whilst Hoechst 33258 staining (blue) highlights nuclei. Images shown are representative images taken with the 20x-objective lens from 24 sites per well. Scale bar in top left corner represents 50 µm. (n = 1).

The receptor expression images (Fig. 12) also appeared to suggest morphological differences between cells. As $G\alpha_{12/13}$ proteins are involved in regulation of the actin cytoskeleton, actin staining (Phalloidin-iFluor 488) and nuclei staining (Hoechst 33258) was carried out using immunocytochemistry techniques (as described in Methods 2.5.3 and 2.5.4). The cellular morphology of the $\Delta G\alpha_{12/13}$ cells seemed to have more cytoskeleton outgrowths compared to the WT cells (Figure 14). The addition of $G\alpha_{12/13}$ proteins to $\Delta G\alpha_{12/13}$ cells appeared to restore the cellular morphology characteristics more like those seen in WT cells (Figure 14).

4 Discussion

The $G\alpha_{12/13}$ class of G proteins is the least studied of the four classes, being the last class to be discovered. This study has made use of several experimental techniques to investigate the role of $G\alpha_{12/13}$ proteins in β-arrestin recruitment at CB_1, including BRET-based biosensor assays. Here, we not only add to previous research investigating $G\alpha_{12/13}$ activation at CB_1, but also present a potentially novel role for $G\alpha_{12/13}$ proteins in modulating CB_1-mediated β-arrestin recruitment. This section discusses the findings of this study in the wider context of the literature on $G\alpha_{12/13}$ protein signalling, with a focus on its effects at CB_1.

4.1 CB_1 activates both $G\alpha_{12}$ and $G\alpha_{13}$ proteins

Using the TRUPATH G protein dissociation assay, we demonstrate that CB_1 can activate both $G\alpha_{12}$ and $G\alpha_{13}$ proteins in HEK293A WT cells. In this assay, three structurally distinct agonists were employed to assess G protein activation – the high potency, high efficacy synthetic cannabinoid AMB-FUBINACA, the partial agonist and phytocannabinoid THC and the allosteric agonist ZCZ-011. Here, all three agonists induced activation of $G\alpha_{12}$ and $G\alpha_{13}$ proteins, with varying efficacy and potency. The promiscuous G protein coupling of CB_1 was further consolidated, through the finding of direct $G\alpha_{12/13}$ coupling to CB_1 in this research. AMB showed the greatest activation of $G\alpha_{12/13}$ proteins, having both high efficacy and high potency at CB_1. Our conclusions are consistent with other findings which demonstrate that AMB has high efficacy when activating the classical CB_1-linked $G\alpha_{i/o}$ class (Gamage et al., 2018). Furthermore, we also found that ZCZ was able to act as an allosteric agonist to activate $G\alpha_{12/13}$ proteins. This adds to the findings by Green et al., (2022), which suggest that the agonist activity of allosteric agonists is largely indistinguishable to orthosteric agonism (Green et al., 2022). Interestingly, the efficacy of $G\alpha_{12}$ activation was lower than $G\alpha_{13}$ activation when stimulated with AMB or ZCZ. However, though we observed a greater BRET $G\alpha_{13}$ signal over

$G\alpha_{12}$, this cannot be assumed to be due to greater dissociation of the tags. BRET-based experiments rely on the presence and proximity of the donor and acceptor tags to produce fluorescence. Therefore, the signal strength can be affected by the levels of expression of each tag, where the presence of all tagged subunits forming the G protein heterotrimer is crucial to the experiment. Furthermore, differences in the structure of the $G\alpha_{12}$ or $G\alpha_{13}$ subunits or position of the tag on each protein could also lead to differences in signal strength, due to the proximity of the donor and acceptor tags being slightly altered. Thus, the observed differences in efficacy could be due to the $G\alpha_{13}$ biosensor having a larger signal-to-noise ratio than the $G\alpha_{12}$ sensor or due to differences in the expression of the $G\alpha_{12}$ / $G\alpha_{13}$ tags. Differences in both would lead to the perception of higher G protein activation.

The coupling of CB_1 to $G\alpha_{12/13}$ proteins has not been studied widely and most studies used downstream effectors to infer G protein activation. Two studies present indirect evidence for $G\alpha_{12/13}$ activation at CB_1, through the use of ROCK inhibitor Y-27362 and $G\alpha_{12/13}$ targeted siRNAs (Ishii & Chun, 2002; Roland et al., 2014). These studies provide indirect evidence of $G\alpha_{12/13}$ activation through measuring downstream effects rather than the G protein activation itself, which our research presents. Consistent with our findings, in a large scale screen of 148 receptors, Inoue et al., (2019) utilised a split luciferase NanoBiT G protein dissociation assay and showed that CB_1 activated $G\alpha_{12/13}$ proteins when stimulated with CP-55940 (Inoue et al., 2019). Inoue et al., (2019) used a G protein coupling score (E_{MAX} / EC_{50}) to assess relative G protein activation, which demonstrated that CB_1 couples to $G\alpha_{12/13}$ proteins, as well as $G\alpha_{i/o}$. Unlike BRET G protein dissociation assays, the NanoBiT assay only measures emissions from the complete luciferase protein when the large and small BiTs are in close proximity (Dixon et al., 2016). Thus, there are no background emissions to interfere with measurement of the signal and efficacy comparisons between sensors are more reliable than BRET-based experiments. In addition, Inoue et al., (2019) made use of a NanoBiT RhoA sensor and confirmed direct

activation of RhoA, an immediate downstream effector of $G\alpha_{12/13}$ proteins, at CB_1 using CP-55940. However, it has been suggested that RhoA can be also activated through other pathways, including by $G\alpha_{q/11}$ (Lutz et al., 2005), which makes it a less reliable indicator of $G\alpha_{12/13}$ activation than direct G protein dissociation.

In most cases where $G\alpha_{12/13}$ protein-receptor coupling has been reported, receptors usually couple to at least one other class of G protein. This is consistent with our findings that confirms $G\alpha_{12/13}$ protein coupling at CB_1, which has been shown to preferentially couple to $G\alpha_{i/o}$ proteins (Bayewitch et al., 1995; Bidaut-Russell et al., 1990; Howlett, 1985). Furthermore, there are many other $G\alpha_{i/o}$ linked receptors which demonstrate this pattern of G protein selectivity, such as the lysophosphatidic acid (LPA) receptor (Mao et al., 1998). In embryonic mouse fibroblast NIH3T3 cells, Mao et al., (1998) used regulators of G protein signalling (RGS) to inhibit $G\alpha_{12/13}$ mediated serum response factor (SRF) activation. This is a key endpoint of $G\alpha_{12/13}$ signalling and LPA receptors were shown to activate $G\alpha_{12/13}$ proteins using G protein inactivation (De Vries et al., 2000). Mao et al., (1998) also utilised a $G\alpha_{q/11}$ deficient cell line to complement their findings, as this class of proteins has been implicated in RhoA activation (Lutz et al., 2005). In addition, the thrombin receptor is another $G\alpha_{i/o}$-linked receptor shown to couple to $G\alpha_{12/13}$ proteins in human platelets, through the use of GTP photo-labelling (Offermanns et al., 1994). In a large scale G protein selectivity study of 148 receptors, 126 of the receptors tested were reported to couple to $G\alpha_{i/o}$ proteins (Inoue et al., 2019). Of these receptors, 52% also demonstrated coupling to $G\alpha_{12/13}$ proteins, suggesting that it is quite common for receptor coupling to multiple G protein families, but poorly studied. Here, our findings add to the promiscuous G protein coupling profile of CB_1, which we find to also include $G\alpha_{12/13}$ proteins.

4.2 $G\alpha_{12/13}$ knock-out enhances β-arrestin recruitment to CB_1

Following confirmation of CB_1 activation of $G\alpha_{12/13}$ proteins, the effect of $G\alpha_{12/13}$ proteins on β-arrestin 2 membrane translocation was investigated. Our findings suggest that CB_1-mediated β-arrestin recruitment is markedly enhanced in HEK293A cells with $G\alpha_{12/13}$ proteins knocked out (Ran et al., 2013) compared wild type cells. This pattern of enhanced β-arrestin recruitment was observed across each of the three agonists used in the G protein dissociation assays (THC, AMB, ZCZ). Upon reintroducing $G\alpha_{12/13}$ proteins to the $G\alpha_{12/13}$ knock-out cells, β-arrestin recruitment was almost abolished, which was consistent across each of the agonists. Like G protein dissociation, AMB demonstrated high potency and efficacy in inducing CB_1-mediated β-arrestin recruitment, whilst THC and ZCZ were much less efficacious.

Our findings suggest that $G\alpha_{12/13}$ proteins are directly involved in inhibiting β-arrestin recruitment mediated by CB_1, through displaying enhanced recruitment in cells lacking $G\alpha_{12/13}$ proteins. Here, we reintroduced $G\alpha_{12/13}$ proteins into $\Delta G\alpha_{12/13}$ cells, potentially resulting in overexpression of these proteins and resulting in an almost-complete abolishment of β-arrestin 2 recruitment. A similar study measured β-arrestin 2 recruitment to vasopressin-2 receptors (V_2R) in HEK293 cells overexpressing $G\alpha_{12}$ proteins (Okashah et al., 2020). Here, Okashah et al., (2020) found that $G\alpha_{12}$ proteins significantly attenuated V_2R-mediated β-arrestin recruitment, correlating with our findings at CB_1. Also consistent with our findings, a recent study discovered that HEK293 $\Delta G\alpha_{12/13}$ cells expressing $G\alpha_{i/q/12}$-coupled free fatty acid receptor 2 (FFA_2) showed moderately increased β-arrestin 2 recruitment (Grundmann et al., 2018). To our knowledge, there is no literature which demonstrates enhanced β-arrestin 2 recruitment at CB_1 in the absence of $G\alpha_{12/13}$ proteins, or attenuated recruitment in their presence. However, both our findings and studies with other receptors demonstrate that $G\alpha_{12/13}$ proteins may have a modulatory role in β-arrestin recruitment at CB_1. Okashah et al., (2020) reported $G\alpha_{12/13}$-V_2R

coupling, but not activation, and inhibited β-arrestin recruitment with $G\alpha_{12/13}$ protein overexpression (Okashah et al., 2020). Okashah et al., (2020) also suggested a competitive interaction between $G\alpha_{12/13}$ proteins and β-arrestin for V_2R. However, our findings at CB_1 suggest that $G\alpha_{12/13}$ proteins are activated, and we reported enhanced β-arrestin recruitment in cells lacking $G\alpha_{12/13}$ proteins. In the absence of $G\alpha_{12/13}$ proteins, reduced competition for CB_1 could explain our discovery of enhanced β-arrestin recruitment.

4.3 $G\alpha_{12/13}$ knock-out leads to attenuation of CB_1-mediated ERK signalling

The phosphorylation of ERK1/2 was investigated as a potential downstream consequence of enhanced β-arrestin recruitment in the absence of $G\alpha_{12/13}$ proteins. Whilst it is accepted that pERK production is governed largely by Gβγ-mediated signalling, β-arrestin has also shown to be important in this pathway (Laprairie et al., 2014). Our findings demonstrated that ERK phosphorylation was almost completely abolished in cells lacking $G\alpha_{12/13}$ proteins compared to wild type. There has been a lack of evidence to support $G\alpha_{12/13}$ inhibition of ERK at CB_1. Our findings could suggest that $G\alpha_{12/13}$ proteins have a potential role in ERK signalling. Interestingly, a previous study demonstrated that over expression of $G\alpha_{12/13}$ proteins may have a role in the inhibition of EGF-mediated ERK activation through sustained stimulation of μ opioid receptors in COS-7 cells (Belcheva et al., 2000). Voyno-Yasenetskaya et al., (1996) also reported that $G\alpha_{12/13}$ proteins inhibit the ERK pathway through inhibition of MEK, which phosphorylates ERK1/2 (Voyno-Yasenetskaya et al., 1996). Honma et al., (2006) suggested that $G\alpha_{12/13}$ proteins cause inhibition of ERK phosphorylation at thromboxane A_2 receptors, using a $G\alpha_{12/13}$ pathway regulator, p115-RGS (Honma et al., 2006). Overall, these findings indicate that the presence of $G\alpha_{12/13}$ proteins leads to inhibition of ERK activation at several receptors. However, our findings suggest that the absence of $G\alpha_{12/13}$ proteins at CB_1 leads to decreased ERK signalling. In our findings, AMB showed the greatest efficacy in ERK

phosphorylation, with ZCZ and THC showing little efficacy. Furthermore, the signalling response in cells with $G\alpha_{12/13}$ proteins reintroduced was particularly poor, even with the positive control for ERK signalling – PMA. Here, transfecting $G\alpha_{12/13}$ proteins was not able to validate the inhibitory effect seen in $\Delta G\alpha_{12/13}$ cells, as it did not rescue the ERK signalling response back to levels seen in WT cells. Instead, the ERK signal was decreased further, even when with the administration of PMA. PMA is a DAG surrogate and stimulates PKC, leading to the activation of the MAPK/ERK pathway (Liu & Heckman, 1998; Ueda et al., 1996). As $G\alpha_{12/13}$ proteins are not likely to be involved in the activation of PKC, this suggests that the ERK response is being affected by other factors. Here, it is possible that cells lacking G proteins could have reduced cellular health or altered biosensor expression; this will be discussed further in the limitations section.

4.4 $G\alpha_{12/13}$ knock-out has no effect on internalisation of CB_1

Since β-arrestin 2 has shown to be crucial in governing receptor desensitisation and internalisation of CB_1 (Jin et al., 1999; Manning et al., 2023), it could be speculated that enhanced β-arrestin recruitment should lead to increased internalisation of CB_1. Thus, this interaction was investigated in cells lacking $G\alpha_{12/13}$ proteins, using THC to stimulate CB_1 internalisation. THC was used instead of a higher efficacy ligand (such as AMB or ZCZ), as the time course kinetics would have been significantly faster and some of the important kinetic data could have been lost. This experiment was only repeated once, so our conclusions need to be verified through repeated experimentation. However, our findings suggest that there are no differences between internalisation kinetics for HEK293A WT cells and those lacking $G\alpha_{12/13}$ proteins. However, the addition of arrestin appeared to shorten the half-life of cell surface CB_1 in both WT and $\Delta G\alpha_{12/13}$ cells as would be expected due to the important role of β-arrestin in

internalisation. However, this experiment was only repeated once due to time constraints and should be repeated to bolster our conclusions.

In comparison to our findings, Okashah et al., (2020) found that cells lacking $G\alpha_{12/13}$ proteins displayed a minor enhancement of V_2R internalisation and significantly attenuated β-arrestin recruitment. This seems to be largely consistent with our conclusions at CB_1. Okashah et al., (2020) also found $G\alpha_{12}$ protein overexpression inhibited V_2R trafficking into endosomes (Okashah et al., 2020). In addition, a recent paper suggested that there was a minor increase in μ-opioid receptor internalisation in HEK293 cells lacking $G\alpha_{12/13}$ proteins (Møller et al., 2023). Interestingly, Shimizu et al., (2017) also suggested that Rho-associated kinase was involved in desensitisation of GPR39 (Shimizu et al., 2017), which typically signals through $G\alpha_{12/13}$, $G\alpha_s$ and $G\alpha_q$ (Holst et al., 2007). Here, Shimizu et al., (2017) discovered that inhibition of the $G\alpha_{12/13}$ signalling pathway using ROCK inhibitor Y-27632 lead to increased GPR39 desensitisation (Shimizu et al., 2017). Our findings suggest that $G\alpha_{12/13}$ proteins have no effect on CB_1 internalisation, though these studies present that $G\alpha_{12/13}$ proteins may be partly involved in desensitisation and internalisation at other receptors. Thus, further investigation into the effect of $G\alpha_{12/13}$ proteins on CB_1 internalisation is needed. The effect of $G\alpha_{12/13}$ on internalisation could be investigated through the overexpression of $G\alpha_{12/13}$ or through administration of ROCK inhibitors in cells expressing CB_1.

As key factors in receptor internalisation, cell surface and total receptor expression was measured using immunocytochemistry, to assess if CB_1 expression was maintained between the WT cells, $\Delta G\alpha_{12/13}$ cells, and $\Delta G\alpha_{12/13}$ cells with $G\alpha_{12/13}$ proteins. Though this experiment was only repeated once, cell surface CB_1 expression was higher in the $\Delta G\alpha_{12/13}$ cells alone, than in the WT cells. Quantification of cell surface CB_1 expression revealed that it was lowest when $G\alpha_{12/13}$ proteins were reintroduced. Furthermore, $\Delta G\alpha_{12/13}$ cells alone had higher total CB_1

expression than WT cells. This seems to suggest that, despite having more total CB_1 in the $\Delta G\alpha_{12/13}$ cells, it is not being trafficked to the cell surface or internalised effectively. Thus, the evident differences in CB_1 expression could distort the conclusions drawn from the BRET-based experiments. Only WT cells were used in the G protein dissociation assay, so conclusions from this experiment remain unaffected. However, the β-arrestin translocation and ERK phosphorylation assays both require receptor stimulation to observe the time course response. Here, the expression levels of the receptor and biosensor need to be compared between cell lines within each assay, with sufficient replication to ascertain the actual effect in each case.

4.5 $G\alpha_{12/13}$ knock-out leads to changes in cell morphology

Interestingly, the immunocytochemistry images appeared to display morphological differences between HEK WT and $\Delta G\alpha_{12/13}$ cells used to assess CB_1 expression. As $G\alpha_{12/13}$ proteins have been shown to be involved in actin cytoskeletal remodelling (Narumiya et al., 1997), we labelled actin with phalloidin to observe differences in cytoskeletal distribution between the cell lines. If this experiment was repeated further, our findings could suggest that $\Delta G\alpha_{12/13}$ cells appear to have more cellular outgrowths than WT cells, which are removed with the reintroduction of $G\alpha_{12/13}$ proteins. This aligns with data suggesting that $G\alpha_{12/13}$ proteins are directly involved in the regulation of actin-rich cellular outgrowths. A previous study presented evidence of a ROCK-mediated pathway which induced Neuro2A cell rounding upon stimulation with AEA (Ishii & Chun, 2002). Consistent with these findings, Roland et al., (2014) observed that $G\alpha_{12/13}$ proteins mediated actin-rich growth cone retraction in hippocampal neurons and Neuro2A cells, through activation of the Rho pathway (Roland et al., 2014). Moreover, Berghuis et al., (2007) also presented that RhoA induced growth cone collapse in cultured rodent interneurons (Berghuis et al., 2007). These studies all seem to support our conclusions that $G\alpha_{12/13}$ proteins are critical in regulation of the cellular projections,

including neurites. Furthermore, $G\alpha_{i/o}$ and $\Delta G\alpha_{12/13}$ proteins may have opposing roles in the regulation of neurite growth. Whilst our findings suggest that $G\alpha_{12/13}$ proteins directly cause the retraction of cellular outgrowths, He et al., (2005) reported that neurite outgrowth was mediated through $G\alpha_{i/o}$ activation of Src in Neuro2A cells (He et al., 2005). Here, as HEK cells are from kidneys rather than neuronal tissue, the cellular outgrowths we observed could be actin-rich processes called lamellipodia or filopodia, which are involved in cell migration and chemotaxis, respectively (Ridley, 2001).

4.6 Limitations and further research

In this research, there were several areas which limit the interpretation of the findings and could be improved with future research. All experiments were conducted using Human Embryonic Kidney cell lines. Their wide use in GPCR research is due to their ease of maintenance and transfection but may not express receptors and proteins in the same manner as neurons. Thus, the cell signalling pathways in HEK cells should be confirmed in neuronal culture to increase biological relevance. Furthermore, whilst knock-out cell lines are useful to examine the effect of signalling inhibition, it may be possible that compensatory remodelling of cellular pathways could occur which might mask the true effect of G protein signalling knock-out. In our study, the addition of $G\alpha_{12/13}$ proteins to the $\Delta G\alpha_{12/13}$ cell line, seems to be an appropriate model of measuring differences in β-arrestin recruitment. However, the inability to rescue the response in the ERK phosphorylation experiment suggests that the effect might not be directly related to $G\alpha_{12/13}$ proteins. This is further supported by the lack of the PMA response in the $\Delta G\alpha_{12/13}$ cells and requires further investigation. In addition, the findings of this research could be distorted by the overall cellular health of the $G\alpha_{12/13}$ knock-out cell lines, though CRISPR/Cas9 genetic editing is highly specific (Naeem et al., 2020). However, a more biologically relevant method of testing receptor signalling pathways could be through using cultured neurons, though these

cells grow incredibly slowly and are difficult to transfect, requiring viral vectors to introduce new DNA. Here, the role of $\Delta G\alpha_{12/13}$ could be investigated using pathway inhibitors, rather than with G protein knock out in neurons. While our study made use of synthetic cannabinoids and a phytocannabinoid, endocannabinoids that could provide a more physiologically relevant method of testing $G\alpha_{12/13}$ activation. Here, unpublished data from the Glass Laboratory investigated G protein dissociation of endocannabinoids AEA and 2-AG at several G proteins, including $G\alpha_{12/13}$. In addition to using endogenous ligands, the use of a RhoA biosensor could provide more evidence elucidating the activation of $G\alpha_{12/13}$ proteins at CB_1. The presence of increased cellular outgrowths in absence of $G\alpha_{12/13}$ proteins also raises an interesting future area for research, which could further investigate the role of CB_1 activation in $G\alpha_{12/13}$-mediated cellular outgrowths.

A key limitation of some of the data was the reduced number of biological repeats (in some cases only one), which severely impacts the reliability of those conclusions. This could be easily remedied through repetition of the necessary experiments to provide a more statistically relevant sample size. In addition, the mechanism through which knock-out of $G\alpha_{12/13}$ proteins enhances CB_1-mediated β-arrestin recruitment is still unknown. Thus, more research into the downstream consequences of enhanced β-arrestin recruitment may shed light on the mechanism through which $G\alpha_{12/13}$ proteins act on this pathway.

4.7 Conclusions

In conclusion, this research has provided evidence to support the limited literature surrounding $G\alpha_{12/13}$ activation at CB_1. This study also presents a potential novel interaction between $G\alpha_{12/13}$ proteins and β-arrestin. Here, β-arrestin recruitment to CB_1 was significantly increased when $G\alpha_{12/13}$ proteins were removed using gene-editing techniques. However, the enhanced β-arrestin recruitment appeared not to increase β-arrestin signalling through ERK1/2 phosphorylation or

CB_1 internalisation. However, the removal of $G\alpha_{12/13}$ proteins appeared to increase the number of cytoskeleton processes emerging from the cells, changing the cellular morphology. Overall, the findings of this study present that $G\alpha_{12/13}$ proteins are activated by CB_1 and, when knocked out, lead to enhanced β-arrestin recruitment to CB_1. However, further studies are needed to fully uncover the mechanism behind and implications of this novel interaction.

References

Ahn, K. H., Mahmoud, M. M., Shim, J.-Y., & Kendall, D. A. (2013). Distinct Roles of β-Arrestin 1 and β-Arrestin 2 in ORG27569-induced Biased Signaling and Internalization of the Cannabinoid Receptor 1 (CB1) *. *Journal of Biological Chemistry*, *288*(14), 9790–9800. https://doi.org/10.1074/jbc.M112.438804

Antoni, F. A. (2012). New paradigms in cAMP signalling. *Molecular and Cellular Endocrinology*, *353*(1), 3–9. https://doi.org/10.1016/j.mce.2011.10.034

Banister, S. D., Longworth, M., Kevin, R., Sachdev, S., Santiago, M., Stuart, J., Mack, J. B. C., Glass, M., McGregor, I. S., Connor, M., & Kassiou, M. (2016). Pharmacology of Valinate and tert-Leucinate Synthetic Cannabinoids 5F-AMBICA, 5F-AMB, 5F-ADB, AMB-FUBINACA, MDMB-FUBINACA, MDMB-CHMICA, and Their Analogues. *ACS Chemical Neuroscience*, *7*(9), 1241–1254. https://doi.org/10.1021/acschemneuro.6b00137

Bayewitch, M., Avidor-Reiss, T., Levy, R., Barg, J., Mechoulam, R., & Vogel, Z. (1995). The peripheral cannabinoid receptor: Adenylate cyclase inhibition and G protein coupling. *FEBS Letters*, *375*(1–2), 143–147. https://doi.org/10.1016/0014-5793(95)01207-U

Belcheva, M. M., Wong, Y. H., & Coscia, C. J. (2000). Evidence for transduction of mu but not kappa opioid modulation of extracellular signal-regulated kinase activity by Gz and G12 proteins. *Cellular Signalling*, *12*(7), 481–489. https://doi.org/10.1016/S0898-6568(00)00095-4

Berghuis, P., Rajnicek, A. M., Morozov, Y. M., Ross, R. A., Mulder, J., Urbán, G. M., Monory, K., Marsicano, G., Matteoli, M., Canty, A., Irving, A. J., Katona, I., Yanagawa, Y., Rakic, P., Lutz, B., Mackie, K., & Harkany, T. (2007). Hardwiring the Brain: Endocannabinoids Shape Neuronal Connectivity. *Science*, *316*(5828), 1212–1216. https://doi.org/10.1126/science.1137406

REFERENCES

Bidaut-Russell, M., Devane, W. A., & Howlett, A. C. (1990). Cannabinoid Receptors and Modulation of Cyclic AMP Accumulation in the Rat Brain. *Journal of Neurochemistry*, *55*(1), 21–26. https://doi.org/10.1111/j.1471-4159.1990.tb08815.x

Bisogno, T., Berrendero, F., Ambrosino, G., Cebeira, M., Ramos, J. A., Fernandez-Ruiz, J. J., & Di Marzo, V. (1999). Brain Regional Distribution of Endocannabinoids: Implications for Their Biosynthesis and Biological Function. *Biochemical and Biophysical Research Communications*, *256*(2), 377–380. https://doi.org/10.1006/bbrc.1999.0254

Bonhaus, D. W., Chang, L. K., Kwan, J., & Martin, G. R. (1998). Dual Activation and Inhibition of Adenylyl Cyclase by Cannabinoid Receptor Agonists: Evidence for Agonist-Specific Trafficking of Intracellular Responses. *Journal of Pharmacology and Experimental Therapeutics*, *287*(3), 884–888.

Bouaboula, M., Poinot-Chazel, C., Bourrié, B., Canat, X., Calandra, B., Rinaldi-Carmona, M., Le Fur, G., & Casellas, P. (1995). Activation of mitogen-activated protein kinases by stimulation of the central cannabinoid receptor CB1. *Biochemical Journal*, *312*(2), 637–641. https://doi.org/10.1042/bj3120637

Buhl, A. M., Johnson, N. L., Dhanasekaran, N., & Johnson, G. L. (1995). Gα12 and Gα13 Stimulate Rho-dependent Stress Fiber Formation and Focal Adhesion Assembly (∗). *Journal of Biological Chemistry*, *270*(42), 24631–24634. https://doi.org/10.1074/jbc.270.42.24631

Calandra, B., Portier, M., Kernéis, A., Delpech, M., Carillon, C., Le Fur, G., Ferrara, P., & Shire, D. (1999). Dual intracellular signaling pathways mediated by the human cannabinoid CB1 receptor. *European Journal of Pharmacology*, *374*(3), 445–455. https://doi.org/10.1016/S0014-2999(99)00349-0

REFERENCES

Daigle, T. L., Kwok, M. L., & Mackie, K. (2008). Regulation of CB1 cannabinoid receptor internalization by a promiscuous phosphorylation-dependent mechanism. *Journal of Neurochemistry*, *106*(1), 70–82. https://doi.org/10.1111/j.1471-4159.2008.05336.x

De Vries, L., Zheng, B., Fischer, T., Elenko, E., & Farquhar, M. G. (2000). The Regulator of G Protein Signaling Family. *Annual Review of Pharmacology and Toxicology*, *40*(1), 235–271. https://doi.org/10.1146/annurev.pharmtox.40.1.235

Delgado-Peraza, F., Ahn, K. H., Nogueras-Ortiz, C., Mungrue, I. N., Mackie, K., Kendall, D. A., & Yudowski, G. A. (2016). Mechanisms of Biased β-Arrestin-Mediated Signaling Downstream from the Cannabinoid 1 Receptor. *Molecular Pharmacology*, *89*(6), 618–629. https://doi.org/10.1124/mol.115.103176

Derkinderen, P., Ledent, C., Parmentier, M., & Girault, J.-A. (2001). Cannabinoids activate p38 mitogen-activated protein kinases through CB1 receptors in hippocampus. *Journal of Neurochemistry*, *77*(3), 957–960. https://doi.org/10.1046/j.1471-4159.2001.00333.x

Derkinderen, P., Valjent, E., Toutant, M., Corvol, J.-C., Enslen, H., Ledent, C., Trzaskos, J., Caboche, J., & Girault, J.-A. (2003). Regulation of Extracellular Signal-Regulated Kinase by Cannabinoids in Hippocampus. *Journal of Neuroscience*, *23*(6), 2371–2382. https://doi.org/10.1523/JNEUROSCI.23-06-02371.2003

DeWire, S. M., Ahn, S., Lefkowitz, R. J., & Shenoy, S. K. (2007). β-Arrestins and Cell Signaling. *Annual Review of Physiology*, *69*(1), 483–510. https://doi.org/10.1146/annurev.physiol.69.022405.154749

Dixon, A. S., Schwinn, M. K., Hall, M. P., Zimmerman, K., Otto, P., Lubben, T. H., Butler, B. L., Binkowski, B. F., Machleidt, T., Kirkland, T. A., Wood, M. G., Eggers, C. T., Encell, L. P., & Wood, K. V. (2016). NanoLuc Complementation Reporter Optimized

for Accurate Measurement of Protein Interactions in Cells. *ACS Chemical Biology*, *11*(2), 400–408. https://doi.org/10.1021/acschembio.5b00753

Dolby, T. W., & Kleinsmith, L. J. (1974). Effects of Δ9-tetrahydrocannabinol on the levels of cyclic adenosine 3',5'-monophosphate in mouse brain. *Biochemical Pharmacology*, *23*(13), 1817–1825. https://doi.org/10.1016/0006-2952(74)90190-7

Donthamsetti, P., Quejada, J. R., Javitch, J. A., Gurevich, V. V., & Lambert, N. A. (2015). Using Bioluminescence Resonance Energy Transfer (BRET) to Characterize Agonist-Induced Arrestin Recruitment to Modified and Unmodified G Protein-Coupled Receptors. *Current Protocols in Pharmacology*, *70*(1), 2.14.1-2.14.14. https://doi.org/10.1002/0471141755.ph0214s70

Duc, N. M., Kim, H. R., & Chung, K. Y. (2015). Structural mechanism of G protein activation by G protein-coupled receptor. *European Journal of Pharmacology*, *763*, 214–222. https://doi.org/10.1016/j.ejphar.2015.05.016

Dupré, D. J., Robitaille, M., Rebois, R. V., & Hébert, T. E. (2009). The Role of Gβγ Subunits in the Organization, Assembly, and Function of GPCR Signaling Complexes. *Annual Review of Pharmacology and Toxicology*, *49*(1), 31–56. https://doi.org/10.1146/annurev-pharmtox-061008-103038

Dutt, P., Nguyen, N., & Toksoz, D. (2004). Role of Lbc RhoGEF in Gα12/13-induced signals to Rho GTPase. *Cellular Signalling*, *16*(2), 201–209. https://doi.org/10.1016/S0898-6568(03)00132-3

Fauré, J., & Dagher, M.-C. (2001). Interactions between Rho GTPases and Rho GDP dissociation inhibitor (Rho-GDI). *Biochimie*, *83*(5), 409–414. https://doi.org/10.1016/S0300-9084(01)01263-9

Felder, C., Joyce, K. E., Briley, E. M., Glass, M., Mackie, K. P., Fahey, K. J., Cullinan, G. J., Hunden, D. C., Johnson, D. W., Chaney, M. O., Koppel, G. A., & Brownstein, M.

(1998). LY320135, a Novel Cannabinoid CB1 Receptor Antagonist, Unmasks Coupling of the CB1 Receptor to Stimulation of cAMP Accumulation. *Journal of Pharmacology and Experimental Therapeutics*, *284*(1), 291–297.

Felder, C., Joyce, K. E., Briley, E. M., Mansouri, J., Mackie, K., Blond, O., Lai, Y., Ma, A. L., & Mitchell, R. L. (1995). Comparison of the pharmacology and signal transduction of the human cannabinoid CB1 and CB2 receptors. *Molecular Pharmacology*, *48*(3), 443–450.

Felder, C., Veluz, J., Williams, H., Briley, E., & Matsuda, L. (1992). Cannabinoid agonists stimulate both receptor- and non-receptor-mediated signal transduction pathways in cells transfected with and expressing cannabinoid receptor clones. *Molecular Pharmacology*, *42*, 838–845.

Finlay, D. B., Cawston, E. E., Grimsey, N. L., Hunter, M. R., Korde, A., Vemuri, V. K., Makriyannis, A., & Glass, M. (2017). Gαs signalling of the CB1 receptor and the influence of receptor number. *British Journal of Pharmacology*, *174*(15), 2545–2562. https://doi.org/10.1111/bph.13866

Finlay, D. B., Manning, J. J., Ibsen, M. S., Macdonald, C. E., Patel, M., Javitch, J. A., Banister, S. D., & Glass, M. (2019). Do Toxic Synthetic Cannabinoid Receptor Agonists Have Signature in Vitro Activity Profiles? A Case Study of AMB-FUBINACA. *ACS Chemical Neuroscience*, *10*(10), 4350–4360. https://doi.org/10.1021/acschemneuro.9b00429

Flores-Otero, J., Ahn, K. H., Delgado-Peraza, F., Mackie, K., Kendall, D. A., & Yudowski, G. A. (2014). Ligand-specific endocytic dwell times control functional selectivity of the cannabinoid receptor 1. *Nature Communications*, *5*(1), Article 1. https://doi.org/10.1038/ncomms5589

REFERENCES

Fukuhara, S., Murga, C., Zohar, M., Igishi, T., & Gutkind, J. S. (1999). A Novel PDZ Domain Containing Guanine Nucleotide Exchange Factor Links Heterotrimeric G Proteins to Rho *. *Journal of Biological Chemistry*, *274*(9), 5868–5879. https://doi.org/10.1074/jbc.274.9.5868

Galve-Roperh, I., Rueda, D., Pulgar, T. G. del, Velasco, G., & Guzmán, M. (2002). Mechanism of Extracellular Signal-Regulated Kinase Activation by the CB1 Cannabinoid Receptor. *Molecular Pharmacology*, *62*(6), 1385–1392. https://doi.org/10.1124/mol.62.6.1385

Gamage, T. F., Anderson, J. C., & Abood, M. E. (2016). CB1 Allosteric Modulator Org27569 Is an Antagonist/Inverse Agonist of ERK1/2 Signaling. *Cannabis and Cannabinoid Research*, *1*(1), 272–280. https://doi.org/10.1089/can.2016.0028

Gamage, T. F., Farquhar, C. E., Lefever, T. W., Marusich, J. A., Kevin, R. C., McGregor, I. S., Wiley, J. L., & Thomas, B. F. (2018). Molecular and Behavioral Pharmacological Characterization of Abused Synthetic Cannabinoids MMB- and MDMB-FUBINACA, MN-18, NNEI, CUMYL-PICA, and 5-Fluoro-CUMYL-PICA. *Journal of Pharmacology and Experimental Therapeutics*, *365*(2), 437–446. https://doi.org/10.1124/jpet.117.246983

Gaoni, Y., & Mechoulam, R. (1964). Isolation, Structure, and Partial Synthesis of an Active Constituent of Hashish. *Journal of the American Chemical Society*, *86*(8), 1646–1647. https://doi.org/10.1021/ja01062a046

Gentry, P. R., Sexton, P. M., & Christopoulos, A. (2015). Novel Allosteric Modulators of G Protein-coupled Receptors *. *Journal of Biological Chemistry*, *290*(32), 19478–19488. https://doi.org/10.1074/jbc.R115.662759

Glass, M., Faull, R. L. M., & Dragunow, M. (1997). Cannabinoid receptors in the human brain: A detailed anatomical and quantitative autoradiographic study in the fetal,

neonatal and adult human brain. *Neuroscience*, *77*(2), 299–318. https://doi.org/10.1016/S0306-4522(96)00428-9

Glass, M., & Felder, C. (1997). Concurrent Stimulation of Cannabinoid CB1 and Dopamine D2 Receptors Augments cAMP Accumulation in Striatal Neurons: Evidence for a Gs Linkage to the CB1 Receptor. *Journal of Neuroscience*, *17*(14), 5327–5333. https://doi.org/10.1523/JNEUROSCI.17-14-05327.1997

Gohla, A., Harhammer, R., & Schultz, G. (1998). The G-protein G13 but Not G12 Mediates Signaling from Lysophosphatidic Acid Receptor via Epidermal Growth Factor Receptor to Rho *. *Journal of Biological Chemistry*, *273*(8), 4653–4659. https://doi.org/10.1074/jbc.273.8.4653

Gómez Del Pulgar, T., Velasco, G., & Guzmán, M. (2000). The CB1 cannabinoid receptor is coupled to the activation of protein kinase B/Akt. *Biochemical Journal*, *347*(2), 369–373. https://doi.org/10.1042/bj3470369

Green, H. M., Finlay, D. B., Ross, R. A., Greig, I. R., Duffull, S. B., & Glass, M. (2022). In Vitro Characterization of 6-Methyl-3-(2-nitro-1-(thiophen-2-yl)ethyl)-2-phenyl-1H-indole (ZCZ011) at the Type 1 Cannabinoid Receptor: Allosteric Agonist or Allosteric Modulator? *ACS Pharmacology & Translational Science*, *5*(12), 1279–1291. https://doi.org/10.1021/acsptsci.2c00160

Grimsey, N. L., Graham, E. S., Dragunow, M., & Glass, M. (2010). Cannabinoid Receptor 1 trafficking and the role of the intracellular pool: Implications for therapeutics. *Biochemical Pharmacology*, *80*(7), 1050–1062. https://doi.org/10.1016/j.bcp.2010.06.007

Grundmann, M., Merten, N., Malfacini, D., Inoue, A., Preis, P., Simon, K., Rüttiger, N., Ziegler, N., Benkel, T., Schmitt, N. K., Ishida, S., Müller, I., Reher, R., Kawakami, K., Inoue, A., Rick, U., Kühl, T., Imhof, D., Aoki, J., … Kostenis, E. (2018). Lack of

beta-arrestin signaling in the absence of active G proteins. *Nature Communications*, *9*(1), Article 1. https://doi.org/10.1038/s41467-017-02661-3

Hains, M. D., Wing, M. R., Maddileti, S., Siderovski, D. P., & Harden, T. K. (2006). Gα12/13- and Rho-Dependent Activation of Phospholipase C-ϵ by Lysophosphatidic Acid and Thrombin Receptors. *Molecular Pharmacology*, *69*(6), 2068–2075. https://doi.org/10.1124/mol.105.017921

Hall, D. A., & Langmead, C. J. (2010). Matching models to data: A receptor pharmacologist's guide. *British Journal of Pharmacology*, *161*(6), 1276–1290. https://doi.org/10.1111/j.1476-5381.2010.00879.x

Hamm, H. E. (1998). The Many Faces of G Protein Signaling *. *Journal of Biological Chemistry*, *273*(2), 669–672. https://doi.org/10.1074/jbc.273.2.669

Harvey, C. D., Ehrhardt, A. G., Cellurale, C., Zhong, H., Yasuda, R., Davis, R. J., & Svoboda, K. (2008). A genetically encoded fluorescent sensor of ERK activity. *Proceedings of the National Academy of Sciences*, *105*(49), 19264–19269. https://doi.org/10.1073/pnas.0804598105

He, J. C., Gomes, I., Nguyen, T., Jayaram, G., Ram, P. T., Devi, L. A., & Iyengar, R. (2005). The Gαo/i-coupled Cannabinoid Receptor-mediated Neurite Outgrowth Involves Rap Regulation of Src and Stat3 *. *Journal of Biological Chemistry*, *280*(39), 33426–33434. https://doi.org/10.1074/jbc.M502812200

Hillard, C. J., Harris, R. A., & Bloom, A. S. (1985). Effects of the cannabinoids on physical properties of brain membranes and phospholipid vesicles: Fluorescence studies. *Journal of Pharmacology and Experimental Therapeutics*, *232*(3), 579–588.

Holst, B., Egerod, K. L., Schild, E., Vickers, S. P., Cheetham, S., Gerlach, L.-O., Storjohann, L., Stidsen, C. E., Jones, R., Beck-Sickinger, A. G., & Schwartz, T. W. (2007).

GPR39 Signaling Is Stimulated by Zinc Ions But Not by Obestatin. *Endocrinology*, *148*(1), 13–20. https://doi.org/10.1210/en.2006-0933

Honma, S., Saika, M., Ohkubo, S., Kurose, H., & Nakahata, N. (2006). Thromboxane A2 receptor-mediated G12/13-dependent glial morphological change. *European Journal of Pharmacology*, *545*(2), 100–108. https://doi.org/10.1016/j.ejphar.2006.06.062

Howlett, A. C. (1985). Cannabinoid inhibition of adenylate cyclase. Biochemistry of the response in neuroblastoma cell membranes. *Molecular Pharmacology*, *27*(4), 429–436.

Howlett, A. C., Qualy, J. M., & Khachatrian, L. L. (1986). Involvement of Gi in the inhibition of adenylate cyclase by cannabimimetic drugs. *Molecular Pharmacology*, *29*(3), 307–313.

Hsieh, C., Brown, S., Derleth, C., & Mackie, K. (1999). Internalization and Recycling of the CB1 Cannabinoid Receptor. *Journal of Neurochemistry*, *73*(2), 493–501. https://doi.org/10.1046/j.1471-4159.1999.0730493.x

Hua, T., Vemuri, K., Nikas, S. P., Laprairie, R. B., Wu, Y., Qu, L., Pu, M., Korde, A., Jiang, S., Ho, J.-H., Han, G. W., Ding, K., Li, X., Liu, H., Hanson, M. A., Zhao, S., Bohn, L. M., Makriyannis, A., Stevens, R. C., & Liu, Z.-J. (2017). Crystal structures of agonist-bound human cannabinoid receptor CB1. *Nature*, *547*(7664), Article 7664. https://doi.org/10.1038/nature23272

Ibsen, M. S., Connor, M., & Glass, M. (2017). Cannabinoid CB1 and CB2 Receptor Signaling and Bias. *Cannabis and Cannabinoid Research*, *2*(1), 48–60. https://doi.org/10.1089/can.2016.0037

Ignatowska-Jankowska, B. M., Baillie, G. L., Kinsey, S., Crowe, M., Ghosh, S., Owens, R. A., Damaj, I. M., Poklis, J., Wiley, J. L., Zanda, M., Zanato, C., Greig, I. R., Lichtman, A. H., & Ross, R. A. (2015). A Cannabinoid CB1 Receptor-Positive

Allosteric Modulator Reduces Neuropathic Pain in the Mouse with No Psychoactive Effects. *Neuropsychopharmacology*, *40*(13), Article 13. https://doi.org/10.1038/npp.2015.148

Inoue, A., Raimondi, F., Kadji, F. M. N., Singh, G., Kishi, T., Uwamizu, A., Ono, Y., Shinjo, Y., Ishida, S., Arang, N., Kawakami, K., Gutkind, J. S., Aoki, J., & Russell, R. B. (2019). Illuminating G-Protein-Coupling Selectivity of GPCRs. *Cell*, *177*(7), 1933-1947.e25. https://doi.org/10.1016/j.cell.2019.04.044

Ishii, I., & Chun, J. (2002). Anandamide-induced neuroblastoma cell rounding via the CB1 cannabinoid receptors. *Neuroreport*, *13*(5), 593–596. https://doi.org/10.1097/00001756-200204160-00011

Jain, R., Watson, U., Vasudevan, L., & Saini, D. K. (2018). Chapter Three—ERK Activation Pathways Downstream of GPCRs. In A. K. Shukla (Ed.), *International Review of Cell and Molecular Biology* (Vol. 338, pp. 79–109). Academic Press. https://doi.org/10.1016/bs.ircmb.2018.02.003

Jin, W., Brown, S., Roche, J. P., Hsieh, C., Celver, J. P., Kovoor, A., Chavkin, C., & Mackie, K. (1999). Distinct Domains of the CB1 Cannabinoid Receptor Mediate Desensitization and Internalization. *Journal of Neuroscience*, *19*(10), 3773–3780. https://doi.org/10.1523/JNEUROSCI.19-10-03773.1999

Kearn, C. S., Blake-Palmer, K., Daniel, E., Mackie, K., & Glass, M. (2005). Concurrent Stimulation of Cannabinoid CB1 and Dopamine D2 Receptors Enhances Heterodimer Formation: A Mechanism for Receptor Cross-Talk? *Molecular Pharmacology*, *67*(5), 1697–1704. https://doi.org/10.1124/mol.104.006882

Kenakin, T. (2007). Allosteric Theory: Taking Therapeutic Advantage of the Malleable Nature of GPCRs. *Current Neuropharmacology*, *5*(3), 149–156. https://doi.org/10.2174/157015907781695973

Khan, S. M., Sleno, R., Gora, S., Zylbergold, P., Laverdure, J.-P., Labbé, J.-C., Miller, G. J., & Hébert, T. E. (2013). The Expanding Roles of Gβγ Subunits in G Protein–Coupled Receptor Signaling and Drug Action. *Pharmacological Reviews*, *65*(2), 545–577. https://doi.org/10.1124/pr.111.005603

Kozasa, T., Jiang, X., Hart, M. J., Sternweis, P. M., Singer, W. D., Gilman, A. G., Bollag, G., & Sternweis, P. C. (1998). P115 RhoGEF, a GTPase activating protein for Gα12 and Gα13. *Science*, *280*(5372), 2109–2111. Scopus. https://doi.org/10.1126/science.280.5372.2109

Krishna Kumar, K., Shalev-Benami, M., Robertson, M. J., Hu, H., Banister, S. D., Hollingsworth, S. A., Latorraca, N. R., Kato, H. E., Hilger, D., Maeda, S., Weis, W. I., Farrens, D. L., Dror, R. O., Malhotra, S. V., Kobilka, B. K., & Skiniotis, G. (2019). Structure of a Signaling Cannabinoid Receptor 1-G Protein Complex. *Cell*, *176*(3), 448-458.e12. https://doi.org/10.1016/j.cell.2018.11.040

Laprairie, R. B., Bagher, A. M., Kelly, M. E. M., Dupré, D. J., & Denovan-Wright, E. M. (2014). Type 1 Cannabinoid Receptor Ligands Display Functional Selectivity in a Cell Culture Model of Striatal Medium Spiny Projection Neurons *. *Journal of Biological Chemistry*, *289*(36), 24845–24862. https://doi.org/10.1074/jbc.M114.557025

Lauckner, J. E., Hille, B., & Mackie, K. (2005). The cannabinoid agonist WIN55,212-2 increases intracellular calcium via CB1 receptor coupling to Gq/11 G proteins. *Proceedings of the National Academy of Sciences*, *102*(52), 19144–19149. https://doi.org/10.1073/pnas.0509588102

Lavoie, H., Gagnon, J., & Therrien, M. (2020). ERK signalling: A master regulator of cell behaviour, life and fate. *Nature Reviews Molecular Cell Biology*, *21*(10), Article 10. https://doi.org/10.1038/s41580-020-0255-7

Liu, W. S., & Heckman, C. A. (1998). The Sevenfold Way of PKC Regulation. *Cellular Signalling*, *10*(8), 529–542. https://doi.org/10.1016/S0898-6568(98)00012-6

Lutz, S., Freichel-Blomquist, A., Yang, Y., Rümenapp, U., Jakobs, K. H., Schmidt, M., & Wieland, T. (2005). The Guanine Nucleotide Exchange Factor p63RhoGEF, a Specific Link between Gq/11-coupled Receptor Signaling and RhoA *. *Journal of Biological Chemistry*, *280*(12), 11134–11139. https://doi.org/10.1074/jbc.M411322200

Mackie, K., & Hille, B. (1992). Cannabinoids inhibit N-type calcium channels in neuroblastoma-glioma cells. *Proceedings of the National Academy of Sciences*, *89*(9), 3825–3829. https://doi.org/10.1073/pnas.89.9.3825

Mackie, K., Lai, Y., Westenbroek, R., & Mitchell, R. (1995). Cannabinoids activate an inwardly rectifying potassium conductance and inhibit Q-type calcium currents in AtT20 cells transfected with rat brain cannabinoid receptor. *Journal of Neuroscience*, *15*(10), 6552–6561. https://doi.org/10.1523/JNEUROSCI.15-10-06552.1995

Manning, J. J., Rawcliffe, G., Finlay, D. B., & Glass, M. (2023). Cannabinoid 1 (CB1) receptor arrestin subtype-selectivity and phosphorylation dependence. *British Journal of Pharmacology*, *180*(3), 369–382. https://doi.org/10.1111/bph.15973

Mao, J., Yuan, H., Xie, W., Simon, M. I., & Wu, D. (1998). Specific Involvement of G Proteins in Regulation of Serum Response Factor-mediated Gene Transcription by Different Receptors *. *Journal of Biological Chemistry*, *273*(42), 27118–27123. https://doi.org/10.1074/jbc.273.42.27118

Matsuda, L. A., Lolait, S. J., Brownstein, M. J., Young, A. C., & Bonner, T. I. (1990). Structure of a cannabinoid receptor and functional expression of the cloned cDNA. *Nature*, *346*(6284), Article 6284. https://doi.org/10.1038/346561a0

Møller, T. C., Moo, E. V., Inoue, A., Pedersen, M. F., & Bräuner-Osborne, H. (2023). Characterization of the real-time internalization of nine GPCRs reveals distinct dependence on arrestins and G proteins. *Biochimica et Biophysica Acta (BBA) - Molecular Cell Research*, *1871*(1), 119584. https://doi.org/10.1016/j.bbamcr.2023.119584

Morrison, D. K. (2012). MAP Kinase Pathways. *Cold Spring Harbor Perspectives in Biology*, *4*(11), a011254. https://doi.org/10.1101/cshperspect.a011254

Munro, S., Thomas, K. L., & Abu-Shaar, M. (1993). Molecular characterization of a peripheral receptor for cannabinoids. *Nature*, *365*(6441), Article 6441. https://doi.org/10.1038/365061a0

Naeem, M., Majeed, S., Hoque, M. Z., & Ahmad, I. (2020). Latest Developed Strategies to Minimize the Off-Target Effects in CRISPR-Cas-Mediated Genome Editing. *Cells*, *9*(7), Article 7. https://doi.org/10.3390/cells9071608

Narumiya, S., Ishizaki, T., & Watanabe, N. (1997). Rho effectors and reorganization of actin cytoskeleton. *FEBS Letters*, *410*(1), 68–72. https://doi.org/10.1016/S0014-5793(97)00317-7

Neves, S. R., Ram, P. T., & Iyengar, R. (2002). G Protein Pathways. *Science*, *296*(5573), 1636–1639. https://doi.org/10.1126/science.1071550

Nobles, K. N., Xiao, K., Ahn, S., Shukla, A. K., Lam, C. M., Rajagopal, S., Strachan, R. T., Huang, T.-Y., Bressler, E. A., Hara, M. R., Shenoy, S. K., Gygi, S. P., & Lefkowitz, R. J. (2011). Distinct Phosphorylation Sites on the β2-Adrenergic Receptor Establish a Barcode That Encodes Differential Functions of β-Arrestin. *Science Signaling*, *4*(185), ra51–ra51. https://doi.org/10.1126/scisignal.2001707

Offermanns, S., Laugwitz, K. L., Spicher, K., & Schultz, G. (1994). G proteins of the G12 family are activated via thromboxane A2 and thrombin receptors in human platelets.

Proceedings of the National Academy of Sciences, *91*(2), 504–508. https://doi.org/10.1073/pnas.91.2.504

Okashah, N., Wright, S. C., Kawakami, K., Mathiasen, S., Zhou, J., Lu, S., Javitch, J. A., Inoue, A., Bouvier, M., & Lambert, N. A. (2020). Agonist-induced formation of unproductive receptor-G12 complexes. *Proceedings of the National Academy of Sciences*, *117*(35), 21723–21730. https://doi.org/10.1073/pnas.2003787117

Olsen, R. H. J., DiBerto, J. F., English, J. G., Glaudin, A. M., Krumm, B. E., Slocum, S. T., Che, T., Gavin, A. C., McCorvy, J. D., Roth, B. L., & Strachan, R. T. (2020). TRUPATH, an open-source biosensor platform for interrogating the GPCR transducerome. *Nature Chemical Biology*, *16*(8), Article 8. https://doi.org/10.1038/s41589-020-0535-8

Pisanti, S., & Bifulco, M. (2019). Medical Cannabis: A plurimillennial history of an evergreen. *Journal of Cellular Physiology*, *234*(6), 8342–8351. https://doi.org/10.1002/jcp.27725

Ran, F. A., Hsu, P. D., Wright, J., Agarwala, V., Scott, D. A., & Zhang, F. (2013). Genome engineering using the CRISPR-Cas9 system. *Nature Protocols*, *8*(11), Article 11. https://doi.org/10.1038/nprot.2013.143

Ridley, A. J. (2001). Rho GTPases and cell migration. *Journal of Cell Science*, *114*(15), 2713–2722. https://doi.org/10.1242/jcs.114.15.2713

Riento, K., & Ridley, A. J. (2003). ROCKs: Multifunctional kinases in cell behaviour. *Nature Reviews Molecular Cell Biology*, *4*(6), Article 6. https://doi.org/10.1038/nrm1128

Roland, A. B., Ricobaraza, A., Carrel, D., Jordan, B. M., Rico, F., Simon, A., Humbert-Claude, M., Ferrier, J., McFadden, M. H., Scheuring, S., & Lenkei, Z. (2014). Cannabinoid-induced actomyosin contractility shapes neuronal morphology and growth. *eLife*, *3*, e03159. https://doi.org/10.7554/eLife.03159

Rümenapp, U., Asmus, M., Schablowski, H., Woznicki, M., Han, L., Jakobs, K. H., Fahimi-Vahid, M., Michalek, C., Wieland, T., & Schmidt, M. (2001). The M3 Muscarinic Acetylcholine Receptor Expressed in HEK-293 Cells Signals to Phospholipase D via G12 but Not Gq-type G Proteins: REGULATORS OF G PROTEINS AS TOOLS TO DISSECT PERTUSSIS TOXIN-RESISTANT G PROTEINS IN RECEPTOR-EFFECTOR COUPLING *. *Journal of Biological Chemistry*, *276*(4), 2474–2479. https://doi.org/10.1074/jbc.M004957200

Sah, V. P., Seasholtz, T. M., Sagi, S. A., & Brown, J. H. (2000). The Role of Rho in G Protein-Coupled Receptor Signal Transduction. *Annual Review of Pharmacology and Toxicology*, *40*(1), 459–489. https://doi.org/10.1146/annurev.pharmtox.40.1.459

Shimizu, Y., Koyama, R., & Kawamoto, T. (2017). Rho kinase-dependent desensitization of GPR39; a unique mechanism of GPCR downregulation. *Biochemical Pharmacology*, *140*, 105–114. https://doi.org/10.1016/j.bcp.2017.06.115

Strathmann, M. P., & Simon, M. I. (1991). G alpha 12 and G alpha 13 subunits define a fourth class of G protein alpha subunits. *Proceedings of the National Academy of Sciences*, *88*(13), 5582–5586. https://doi.org/10.1073/pnas.88.13.5582

Sugimoto, N., Takuwa, N., Okamoto, H., Sakurada, S., & Takuwa, Y. (2003). Inhibitory and Stimulatory Regulation of Rac and Cell Motility by the G12/13-Rho and Gi Pathways Integrated Downstream of a Single G Protein-Coupled Sphingosine-1-Phosphate Receptor Isoform. *Molecular and Cellular Biology*, *23*(5), 1534–1545. https://doi.org/10.1128/MCB.23.5.1534-1545.2003

Sugiura, T., Kodaka, T., Kondo, S., Tonegawa, T., Nakane, S., Kishimoto, S., Yamashita, A., & Waku, K. (1996). 2-Arachidonoylglycerol, a Putative Endogenous Cannabinoid Receptor Ligand, Induces Rapid, Transient Elevation of Intracellular Free Ca2+in

Neuroblastoma × Glioma Hybrid NG108-15 Cells. *Biochemical and Biophysical Research Communications*, *229*(1), 58–64. https://doi.org/10.1006/bbrc.1996.1757

Sugiura, T., Kodaka, T., Kondo, S., Tonegawa, T., Nakane, S., Kishimoto, S., Yamashita, A., & Waku, K. (1997). Inhibition by 2-Arachidonoylglycerol, a Novel Type of Possible Neuromodulator, of the Depolarization-Induced Increase in Intracellular Free Calcium in Neuroblastoma × Glioma Hybrid NG108-15 Cells. *Biochemical and Biophysical Research Communications*, *233*(1), 207–210. https://doi.org/10.1006/bbrc.1997.6425

Syrovatkina, V., Alegre, K. O., Dey, R., & Huang, X.-Y. (2016). Regulation, Signaling, and Physiological Functions of G-Proteins. *Journal of Molecular Biology*, *428*(19), 3850–3868. https://doi.org/10.1016/j.jmb.2016.08.002

Treisman, R., Alberts, A. S., & Sahai, E. (1998). Regulation of SRF Activity by Rho Family GTPases. *Cold Spring Harbor Symposia on Quantitative Biology*, *63*, 643–652. https://doi.org/10.1101/sqb.1998.63.643

Ueda, Y., Hirai, S., Osada, S., Suzuki, A., Mizuno, K., & Ohno, S. (1996). Protein Kinase C δ Activates the MEK-ERK Pathway in a Manner Independent of Ras and Dependent on Raf *. *Journal of Biological Chemistry*, *271*(38), 23512–23519. https://doi.org/10.1074/jbc.271.38.23512

Voyno-Yasenetskaya, T. A., Faure, M. P., Ahn, N. G., & Bourne, H. R. (1996). Gα12 and Gα13 Regulate Extracellular Signal-regulated Kinase and c-Jun Kinase Pathways by Different Mechanisms in COS-7 Cells *. *Journal of Biological Chemistry*, *271*(35), 21081–21087. https://doi.org/10.1074/jbc.271.35.21081

Appendices

Table 10. General equipment, reagents and drugs used.

Item	Source	Catalogue Number
(-)-*trans*-Δ9-tetrahydrocannabinol (THC) (Ethanol vehicle)	Toronto Research Chemicals Inc. (Toronto, Canada)	T293225
AlbumiNZ™ Bovine Albumin Low Free Fatty Acid (BSA)	MP Biomedicals (Auckland, NZ)	199899
Alexa Fluor® 488 goat anti-mouse IgG (H+L) antibody	Thermo Fisher Scientific (Waltham, MA, USA)	A11029
Coelenterazine 400a	Nanolight Technology (Pinetop, AZ, USA)	340
Coelenterazine-h	Nanolight Technology (Pinetop, AZ, USA)	301
Corning® 100 mm TC-treated Culture Dish	Corning (Corning, New York, NY, USA)	430167
Corning® 6-well Clear Cell Culture Treated Microplates	Corning (Corning, New York, NY, USA)	CORN3516
Corning® Cell Culture Flask 75 cm^2 rectangular canted neck cell culture flasks with vent caps	Corning (Corning, New York, NY, USA)	430641U
Corning® Costar® 96-well Clear Flat Bottom Polystyrene TC-Treated Microplates	Corning (Corning, New York, NY, USA)	3596
Corning® Costar® 96-well White Opaque Flat Bottom Polystyrene TC-Treated Microplates	Corning (Corning, New York, NY, USA)	CORN3917
CulturPlate™ 96 white opaque 96-well microplate, sterile and tissue culture treated	PerkinElmer (Waltham MA, USA)	6005689
Dimethyl Sulfoxide (DMSO)	Sigma-Aldrich (St Louis, MO, USA)	276855
Dulbecco's Modified Eagle Medium (no-phenol red, high glucose, pyruvate, HEPES)	Thermo Fisher Scientific (Waltham, MA, USA)	21063029
Dulbecco's Modified Eagle Medium (phenol-red, high glucose, pyruvate)	Thermo Fisher Scientific (Waltham, MA, USA)	11995073
Ethanol absolute	Lab Supply (Dunedin, NZ)	CHE2292.1

Ethylmercurithiosalicylic acid, sodium salt (Thiomersal/merthiolate)	Thermo Fisher Scientific (Waltham, MA, USA)	ACR118680250
Foetal bovine serum (FBS)	Moregate Biotech (Brisbane, Australia)	FBSF
Hoechst 33258	Life Tech, Eugene, OR, USA	H1398
LUMIstar® Omega Plate Reader	BMG Labtech GmbH, Ortenberg, Germany	-
Methyl (2S)-2-{[1-[(4-fluorophenyl)methyl]indazole-3-carbonyl]amino}-3-methylbutanoate (AMB-FUBINACA) (DMSO vehicle)	Cayman Chemical Company (Ann Arbor, MI, USA)	9001960
Opti-MEM™ reduced serum medium	Thermo Fisher Scientific (Waltham, MA, USA)	31985062
Paraformaldehyde (PFA)	Thermo Fisher Scientific (Waltham, MA, USA)	ACR416780010
Phalloidin-iFluor 488	Gifted from Wise Lab (Abcam)	AB176753
Phorbol-12-myristate-13-acetate (PMA)	Cayman Chemical Company (Ann Arbor, MI, USA)	10008014
Poly-D-Lysine hydrobromide (PDL)	Sigma-Aldrich (St Louis, MO, USA)	P1149
Polyethyleneimine 40 kDa (PEI Max)	Polysciences (Warrington, MA, USA)	24765
Primary mouse monoclonal anti-HA.11 IgG (clone 16B12)	BioLegend (San Diego, CA, USA)	901503
Triton™ X100	Sigma-Aldrich (St Louis, MO, USA)	X100-500ML
TRUPATH Biosensors (Gα12-/Gα13-Rluc8, Gβ3, Gγ9-GFP2)	Gifted from Bryan Roth (Addgene, MA, USA)	Kit #1000000163
Trypan Blue Solution	Thermo Fisher Scientific (Waltham, MA, USA)	15250061
Trypsin-EDTA (0.05%, phenol red)	Thermo Fisher Scientific (Waltham, MA, USA)	25300062
ZCZ-011 (DMSO vehicle)	Gifted from Professor Ruth Ross	-